Constraints on *CP*-violating gauge-Higgs operators

Siddharth Dwivedi,[1,*] Dilip Kumar Ghosh,[2,†] Biswarup Mukhopadhyaya,[1,‡] and Ambresh Shivaji[1,§]

[1]*Regional Centre for Accelerator-based Particle Physics, Harish-Chandra Research Institute,*
Chhatnag Road, Jhunsi, Allahabad 211019, India
[2]*Department of Theoretical Physics, Indian Association for the Cultivation of Science,*
2A & 2B Raja S.C. Mullick Road, Kolkata 700032, India

We consider the most general set of $SU(2) \times U(1)$ invariant *CP*-violating operators of dimension six, which contribute to VVh interactions ($V = W, Z, \gamma$). Our aim is to constrain any *CP*-violating new physics above the electroweak scale via the effective couplings that arise when such physics is integrated out. For this purpose, we use, in turn, electroweak precision data, global fits of Higgs data at the Large Hadron Collider and the electric dipole moments of the neutron and the electron. We thus impose constraints mainly on two-parameter and three-parameter spaces. We find that the constraints from the electroweak precision data are the weakest. Among the existing Higgs search channels, considerable constraints come from the diphoton signal strength. We note that potential contribution to $h \to \gamma Z$ may in principle be a useful constraining factor, but it can be utilized only in the high energy run. The contributions to electric dipole moments mostly lead to the strongest constraints, though somewhat fine-tuned combinations of more than one parameter with large magnitudes are allowed. We also discuss constraints on gauge boson trilinear couplings which depend on the parameters of the *CP*-violating operators.

PACS numbers: 12.60.-i, 14.80.Bn, 12.60.Fr

I. INTRODUCTION

Although the discovery of "a Higgs-like boson" at the Large Hadron Collider (LHC) has been a refreshing development [1,2], there is no clear signal yet for physics beyond the standard model (SM). It is therefore natural that physicists are trying to wring the last drop out of the Higgs sector itself, in attempts to read fingerprints of new physics.

One approach is to examine all available data in terms of specific new models, such as supersymmetry or just additional Higgs doublets. In the other approach, one can take a model-independent stance, parametrize possible modifications of the interaction terms of the Higgs with pairs of SM particles, and examine them in the light of the available data. Such modifications can again be of two types. In the first category, they are just multiplicative modifications of the coupling strengths, the Lorentz structures remaining the same as in the SM. Constraints on such modifications have already been derived from the available Higgs data [3–7]. In the second class, one considers additional operators with new Lorentz structures satisfying all symmetries of the SM [8–15]. Gauge invariance of such operators in their original forms may be expected, since they are obtained by integrating out new physics that is just above the reach of the present round of experiments. Sets of such higher-dimensional operators contributing to the effective coupling of the Higgs to, say a pair of electroweak vector

bosons have been studied extensively. Here it makes sense to include only $SU(2) \times U(1)$ invariant operators in one's list to start with, because the yet unknown new physics lies at least a little above the electroweak symmetry breaking scale. A host of such gauge invariant higher-dimensional operators have been, and are being, analyzed with considerable rigor, and now there exist limits on them, using data ranging from electroweak precision measurements to global fits of LHC results [16–49].

Most of such analyses include higher-dimensional operators that conserve charge conjugation (*C*), parity (*P*) and time-reversal (*T*). However, there is evidence of *C*, *P* and *CP*-violation in weak interactions [50], and there are speculations about other sources of *CP*-violation as well, especially with a view to explaining the baryon asymmetry in our universe [51,52]. The possibility of *CP*-nonconservation cannot therefore be ruled out in the new physics currently sought after. Thus one may in principle also obtain higher-dimensional interaction terms involving the Higgs and a pair of gauge bosons. The constraints on such terms, and identification of regions in the parameter space where they can be phenomenologically significant, form the subject-matter of the present paper.

The *CP*-violating effective couplings, interestingly, are not constrained by the oblique electroweak parameters at one-loop level up to $\mathcal{O}(\frac{1}{\Lambda^2})$, where Λ is the cutoff scale of the effective theory. The leading contributions to self-energy corrections to electroweak gauge bosons at one-loop level occur at $\mathcal{O}(\frac{1}{\Lambda^4})$. Therefore, electroweak precision (EWP) data are not expected to provide severe constraints on *CP*-odd parameters. In addition to this, Higgs-mediated

*[*]siddharthdwivedi@hri.res.in
[†]tpdkg@iacs.res.in
[‡]biswarup@hri.res.in
[§]ambreshkshivaji@hri.res.in

event rates in various channels receive contributions from these couplings at $\mathcal{O}(\frac{1}{\Lambda^4})$. Thus they can also be constrained from global fits of the LHC data. The strongest limits on them, however, arise from the contributions to the electric dipole moments (EDMs) of the neutron and the electron, both of which are severely restricted from experiments. As we shall see in the following sections, a single *CP*-violating operator taken at a time may in certain cases be limited to a very small strength from the above constraints, while two or three such operators considered together can have relatively larger, but highly correlated coefficients. Some of these operators can have interesting phenomenological implications, especially in the context of the LHC.

A study in similar lines can be found in Refs. [42, 45–47,49]. However, we have performed the most comprehensive analysis, taking all the five possible dimension-6 *CP*-violating *VVh* operators ($V = W, Z, \gamma$), which are not yet discussed thoroughly in the literature. We provide the constraints obtained from the oblique electroweak parameters. The constraints coming from global fits of LHC data and electric dipole moments, for two and three operators taken at a time, have been compared. In addition to these we also provide the constraints on trilinear gauge boson couplings coming from LEP data on gauge boson pair production.

Our paper is organized as follows. In Sec. II, we provide details on the *CP*-violating gauge Higgs operators and derive Feynman rules for three point vertices of our interest. In Sec. III we present the constraints on *CP*-violating parameters coming from the precision electroweak measurements. Following this, we perform a global analysis of these parameters using LHC data on Higgs in Sec. IV and we discuss EDM constraints on *CP*-violating parameters in Sec. V. Section VI is devoted to discussion of results. Finally we summarize and conclude in Sec. VII.

II. MORPHOLOGY OF *CP*-VIOLATING GAUGE-HIGGS OPERATORS

In the effective Lagrangian approach that has been followed here, one can write a Lagrangian ($\mathcal{L}_{\mathrm{eff}}$) comprising only of the SM fields, where the effects of the new physics that appear above the cutoff scale Λ are encapsulated in higher dimensional gauge invariant operators. In general,

$$\mathcal{L}_{\mathrm{eff}} = \sum_i \frac{f_i}{\Lambda^{d_i-4}} O^i, \tag{1}$$

where $d_i > 4$ is the mass dimension of the operator O^i and the dimensionless free parameter f_i fixes the strength of the corresponding operator. The operators constructed out of the Higgs doublet and the $SU(2) \times U(1)$ gauge fields are of even dimensions, and at the leading order they have mass dimension $d_i = 6$. The dimension six *CP*-even gauge invariant operators constructed out of the Higgs doublet

(Φ) and the electroweak gauge fields (B_μ, W_μ^a), that modify the gauge-Higgs couplings are given as follows:

$$O_W = \frac{f_W}{\Lambda^2}(D_\mu\Phi)^\dagger \hat{W}^{\mu\nu}(D_\nu\Phi); \quad O_B = \frac{f_B}{\Lambda^2}(D_\mu\Phi)^\dagger \hat{B}^{\mu\nu}(D_\nu\Phi);$$

$$O_{BB} = \frac{f_{BB}}{\Lambda^2}\Phi^\dagger \hat{B}^{\mu\nu}\hat{B}_{\mu\nu}\Phi; \qquad O_{WW} = \frac{f_{WW}}{\Lambda^2}\Phi^\dagger \hat{W}^{\mu\nu}\hat{W}_{\mu\nu}\Phi;$$

$$O_{BW} = \frac{f_{BW}}{\Lambda^2}\Phi^\dagger \hat{B}^{\mu\nu}\hat{W}_{\mu\nu}\Phi. \tag{2}$$

In the above, we have defined $\hat{B}_{\mu\nu} = i\frac{g'}{2}B_{\mu\nu}$ and $\hat{W}_{\mu\nu} = i\frac{g}{2}\tau^a W_{\mu\nu}^a$. g and g' are the electroweak coupling parameters corresponding to $SU(2)$ and $U(1)$ gauge groups respectively, and $\tau^a(a = 1, 2, 3)$ are the three Pauli matrices. We define the gauge covariant derivative as $D_\mu \equiv \partial_\mu - i\frac{g}{2}\tau^a W_\mu^a - i\frac{g'}{2}YB_\mu$, where Y is the hypercharge quantum number. With this choice of the definition of gauge covariant derivative, field strength tensor $W_{\mu\nu}^a$ is given by, $W_{\mu\nu}^a = \partial_\mu W_\nu^a - \partial_\nu W_\mu^a + g\epsilon^{abc}W_\mu^b W_\nu^c$. The constraints on *CP*-even parameters and their collider implications have been studied extensively in the literature [16,21,32,36,43,44,48]. In this work we are interested in corresponding *CP*-violating dimension six gauge-Higgs operators. These are,

$$\tilde{O}_W = \frac{\tilde{f}_W}{\Lambda^2}(D_\mu\Phi)^\dagger \hat{\tilde{W}}^{\mu\nu}(D_\nu\Phi); \quad \tilde{O}_B = \frac{\tilde{f}_B}{\Lambda^2}(D_\mu\Phi)^\dagger \hat{\tilde{B}}^{\mu\nu}(D_\nu\Phi);$$

$$\tilde{O}_{BB} = \frac{\tilde{f}_{BB}}{\Lambda^2}\Phi^\dagger \hat{B}^{\mu\nu}\hat{\tilde{B}}_{\mu\nu}\Phi; \qquad \tilde{O}_{WW} = \frac{\tilde{f}_{WW}}{\Lambda^2}\Phi^\dagger \hat{\tilde{W}}^{\mu\nu}\hat{W}_{\mu\nu}\Phi;$$

$$\tilde{O}_{BW} = \frac{\tilde{f}_{BW}}{\Lambda^2}\Phi^\dagger \hat{\tilde{B}}^{\mu\nu}\hat{W}_{\mu\nu}\Phi, \tag{3}$$

where, $\hat{\tilde{W}}^{\mu\nu} = \frac{1}{2}\epsilon^{\mu\nu\alpha\beta}\hat{W}_{\alpha\beta}$ and $\hat{\tilde{B}}^{\mu\nu} = \frac{1}{2}\epsilon^{\mu\nu\alpha\beta}\hat{B}_{\alpha\beta}$, $\epsilon^{\mu\nu\alpha\beta}$ being the four-dimensional fully antisymmetric tensor with $\epsilon^{0123} = 1$.

In principle, the *CP*-even operators [Eq. (2)] could have been assumed to exist simultaneously with the *CP*-odd ones considered here. However, such an approach generates far too large a set of free parameters, where the signature of the *CP*-violating effective couplings would be drowned. Moreover, the *CP*-even operators are independent of the *CP*-odd ones (and vice versa); therefore, setting them to zero is a viable phenomenological approach. We therefore postulate that the new physics above scale Λ is such that *only CP-violating dimension six effective operators are appreciable*, and the corresponding *CP*-conserving ones are much smaller. Such a "simplified approach," we reiterate, is unavoidable for unveiling *CP*-violating high scale physics, as has been recognized in the literature [49,53–55]. Studies focusing exclusively on the generation of *CP*-violating terms in specific new physics frameworks can also be found, an example being those in the context of extra space-time dimensions [56,57].

TABLE I.   *CP*-odd *VVh* and *WWV* coupling factors and their effective strengths.

Coupling	Effective coupling strength
C_{WWh}	$(-\tilde{f}_W - 2\tilde{f}_{WW})$
C_{ZZh}	$-1/c_W^2[c_W^2\tilde{f}_W + s_W^2\tilde{f}_B + 2(c_W^4\tilde{f}_{WW} + s_W^4\tilde{f}_{BB}) + 2s_W^2 c_W^2\tilde{f}_{BW}]$
$C_{\gamma\gamma h}$	$-2s_W^2(\tilde{f}_{WW} + \tilde{f}_{BB} - \tilde{f}_{BW})$
$C_{\gamma Zh}$	$t_W/2[(-\tilde{f}_W + \tilde{f}_B) + 4(s_W^2\tilde{f}_{BB} - c_W^2\tilde{f}_{WW}) + 2c_{2W}\tilde{f}_{BW}]$
$C_{WW\gamma}$	$s_W/2(\tilde{f}_W + \tilde{f}_B + 2\tilde{f}_{BW})$
C_{WWZ}	$-s_W t_W/2(\tilde{f}_W + \tilde{f}_B + 2\tilde{f}_{BW})$

Since we focus on the extension of the SM through the inclusion of the *CP*-odd operators only, the full BSM Lagrangian looks like,

$$\mathcal{L}_{\text{BSM}} = \mathcal{L}_{\text{SM}} + \tilde{O}_W + \tilde{O}_{WW} + \tilde{O}_B + \tilde{O}_{BB} + \tilde{O}_{BW}, \quad (4)$$

where $\mathcal{L}_{\text{SM}}$ is the standard model Lagrangian. After the electroweak symmetry breaking, these *CP*-odd operators contribute to following three-point vertices of our interest,[1]

$$\mathcal{L}_{WWh} = -\frac{gm_W}{\Lambda^2}(\tilde{f}_W + 2\tilde{f}_{WW})$$
$$\times \epsilon^{\mu\nu\alpha\beta}k_{1\alpha}k_{2\beta}W_\mu^+(k_1)W_\nu^-(k_2)h(k), \quad (5)$$

$$\mathcal{L}_{ZZh} = -\frac{gm_W}{\Lambda^2}\left[\frac{c_W^2\tilde{f}_W + s_W^2\tilde{f}_B}{c_W^2} + \frac{2(c_W^4\tilde{f}_{WW} + s_W^4\tilde{f}_{BB})}{c_W^2}\right.$$
$$\left. + 2s_W^2\tilde{f}_{BW}\right]\epsilon^{\mu\nu\alpha\beta}k_{1\alpha}k_{2\beta}Z_\mu(k_1)Z_\nu(k_2)h(k), \quad (6)$$

$$\mathcal{L}_{\gamma\gamma h} = -2\left(\frac{gm_W}{\Lambda^2}\right)s_W^2(\tilde{f}_{WW} + \tilde{f}_{BB} - \tilde{f}_{BW})$$
$$\times \epsilon^{\mu\nu\alpha\beta}k_{1\alpha}k_{2\beta}A_\mu(k_1)A_\nu(k_2)h(k), \quad (7)$$

$$\mathcal{L}_{\gamma Zh} = \left(\frac{gm_W}{2\Lambda^2}\right)t_W[(-\tilde{f}_W + \tilde{f}_B) + 4(s_W^2\tilde{f}_{BB} - c_W^2\tilde{f}_{WW})$$
$$+ 2c_{2W}\tilde{f}_{BW}]\epsilon^{\mu\nu\alpha\beta}k_{1\alpha}k_{2\beta}A_\mu(k_1)Z_\nu(k_2)h(k), \quad (8)$$

$$\mathcal{L}_{WW\gamma} = \left(\frac{gm_W^2}{2\Lambda^2}\right)s_W(\tilde{f}_W + \tilde{f}_B + 2\tilde{f}_{BW})$$
$$\times \epsilon^{\mu\nu\alpha\beta}k_\beta W_\mu^+(k_1)W_\nu^-(k_2)A_\alpha(k), \quad (9)$$

$$\mathcal{L}_{WWZ} = -\left(\frac{gm_W^2}{2\Lambda^2}\right)(s_W t_W)(\tilde{f}_W + \tilde{f}_B + 2\tilde{f}_{BW})$$
$$\times \epsilon^{\mu\nu\alpha\beta}k_\beta W_\mu^+(k_1)W_\nu^-(k_2)Z_\alpha(k). \quad (10)$$

In the above equations $s_W = \sin\theta_W$, $c_W = \cos\theta_W$, $t_W = \tan\theta_W$, and $c_{2W} = \cos 2\theta_W$, where θ_W is the Weinberg angle. Here *k*s are the four-momenta of the fields that enter the vertex. We have taken all momenta to be inflowing toward the three-point vertex in establishing the Feynman rules. From the list of *CP*-odd interaction vertices shown above, one can observe a general tensor structure of the form $\epsilon^{\mu\nu\alpha\beta}k_{1\alpha}k_{2\beta}$ in *VVh* vertices and a general tensor structure of the form $\epsilon^{\mu\nu\alpha\beta}k_\beta$ in trilinear gauge boson couplings (*WWV*). Because of this the *CP*-odd couplings are linear combinations of the parameters $\tilde{f}_i$. Note that we have not included the *CP*-odd operator involving gluon-Higgs coupling,

$$\tilde{O}_{GG} = \frac{\tilde{f}_{GG}}{\Lambda^2}\Phi^\dagger\hat{\tilde{G}}^{\mu\nu}\hat{G}_{\mu\nu}\Phi. \quad (11)$$

This operator introduces a θ_{QCD} term [58,59], and it is severely constrained by the experimental measurement of neutron EDM [50]. In Table I, we list various couplings and their effective strengths ignoring the overall dimension full factor of $\frac{gm_W}{\Lambda^2}$ in C_{VVh} and the dimensionless factor of $\frac{gm_W^2}{\Lambda^2}$ in C_{WWV} couplings. Note that only *ZZh* and *γZh* couplings receive contribution from all five *CP*-odd operators. The operators which contribute to *WWγ* also contribute to *WWZ* and these couplings are related by, $C_{WWZ} = -t_W C_{WW\gamma}$.

III. CONSTRAINTS FROM ELECTROWEAK PRECISION (EWP) DATA

We note that unlike some of the *CP*-even (D = 6) operators, the *CP*-odd operators do not contribute to the gauge boson propagator corrections at tree level, hence are not expected to receive severe bounds from the electroweak precision data. This is due to the antisymmetry of the epsilon tensor which is present in all *CP*-odd operators. In fact, because of the same reason, all quantum corrections to gauge boson two-point functions up to $\mathcal{O}(\frac{1}{\Lambda^2})$ vanish[2] and first nonzero contributions due to *CP*-odd operators appear

---

[1]The *CP*-odd operators considered here also contribute to four-point and five-point vertices like *VVhh*, *VVVh* and *VVVhh*. However, as we will see in following sections, all the observables used in our analysis are sensitive to only three-point vertices at the leading order.

[2]These corrections are proportional to $\epsilon^{\mu\nu\alpha\beta}p_\alpha p_\beta$ (*p* being the four-momentum of gauge boson) which is zero.
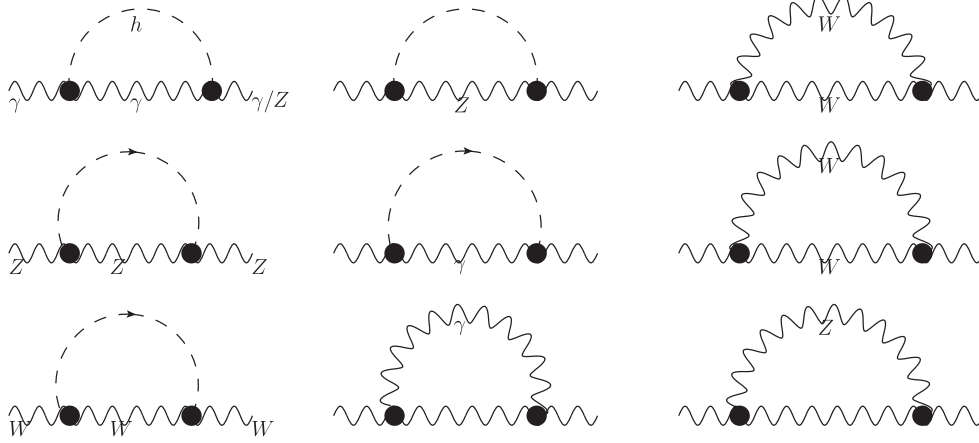
FIG. 1.   One-loop self energy corrections to electroweak vector bosons (oblique corrections) in presence of *CP*-odd operators. The blobs show the effective *CP*-odd vertices. These corrections are of $\mathcal{O}(1/\Lambda^4)$.

at $\mathcal{O}(\frac{1}{\Lambda^4})$. As we will see in Sec. IV, the *CP*-odd couplings contribute to observables related to LHC Higgs data at this order. It would be interesting to discuss the implications of the electroweak precision measurement constraints on the parameters of *CP*-odd operators.

It is well known that the dominant effects of new physics can be conveniently parametrized in terms of Peskin-Takeuchi parameters [60]. These are related to the gauge boson two-point functions as,

$$\alpha S = 4c_W^2 s_W^2 \left(\Pi_{ZZ}'(0) - \Pi_{\gamma\gamma}'(0) - \frac{c_W^2 - s_W^2}{s_W c_W} \Pi_{\gamma Z}'(0) \right) \quad (12)$$

$$\alpha T = \frac{\Pi_{WW}(0)}{m_W^2} - \frac{\Pi_{ZZ}(0)}{m_Z^2} \quad (13)$$

$$\alpha U = 4s_W^2 (\Pi_{WW}'(0) - c_W \Pi_{ZZ}'(0) - s_W^2 \Pi_{\gamma\gamma}'(0) - 2c_W s_W \Pi_{\gamma Z}'(0)) \quad (14)$$

where, $\Pi_{V_1 V_2}(p^2)$ and $\Pi_{V_1 V_2}'(p^2)$ are the $g^{\mu\nu}$ part of the two-point function and its derivative with respect to p^2, respectively. The relevant one-loop Feynman diagrams are shown in Fig. 1. We have regularized ultraviolet (UV) singularities of these diagrams in dimensional regularization (DR). The expressions for $\Pi_{V_1 V_2}(p^2)$ in terms of standard one-loop scalar functions are given in Appendix A. We find that $\Pi_{\gamma\gamma}(0) = \Pi_{\gamma Z}(0) = 0$ which is expected due to the transverse nature of the photon. The renormalization of UV singularity is carried out in $\overline{\text{MS}}$ scheme which introduces scale dependence in these expressions. We have identified the renormalization scale with the cutoff scale Λ. Thus the gauge boson two-point functions also have $\ln(\Lambda)$ dependence apart from the overall $1/\Lambda^4$ dependence coming from *CP*-odd couplings. Because of this an explicit choice of Λ is necessary in deriving the EWP constraints on $\tilde{f}_i$s.

For $\Lambda = 1$ TeV, the Peskin-Takeuchi parameters due to *CP*-odd couplings are given by,

$$S = (-3.36C_{\gamma\gamma h}^2 - 1.28C_{\gamma Z h}^2 + 4.64C_{ZZh}^2 \\ - 4.49C_{\gamma\gamma h}C_{\gamma Z h} - 6.21C_{\gamma Z h}C_{ZZh}) \times 10^{-5} \quad (15)$$

$$T = -9.74 \times 10^{-5} C_{WW\gamma}^2 \quad (16)$$

$$U = (-0.960C_{\gamma\gamma h}^2 - 4.69C_{\gamma Z h}^2 - 4.64C_{ZZh}^2 + 5.67C_{WWh}^2 \\ + 2.76C_{WW\gamma}^2 - 3.59C_{\gamma\gamma h}C_{\gamma Z h} - 4.96C_{\gamma Z h}C_{ZZh}) \times 10^{-5}. \quad (17)$$

We can also express them in terms of $\tilde{f}_i$s using their relation with C_is given in Table I. The experimental limits on S, T and U parameters are obtained by fitting the data on various electroweak observables with these parameters. The limits are [50],

$$S = -0.03 \pm 0.10, \qquad T = 0.01 \pm 0.12, \\ U = 0.05 \pm 0.10. \quad (18)$$

In Eqs. (15), (16) and (17) the coefficients of various couplings are $\sim 10^{-5}$ suggesting that the EWP constraints cannot be very strong. Therefore, we only consider the case where any two out of five parameters are nonzero. In Fig. 2, we display the allowed range for *CP*-odd parameters which satisfy the above limits on S, T and U parameters for all ten sets of two parameters taken together. Here we have varied parameters freely to ensure that we obtain a bounded region. We note that large values of $\mathcal{O}(1000)$ for $\tilde{f}_{BB}$ are always allowed. On the other hand the allowed range for $\tilde{f}_{WW}$ never goes beyond 250. Allowed values for all other parameters can be of $\mathcal{O}(100-1000)$. Some of these observations can be understood once we express the S, T and U parameters in terms of $\tilde{f}_i$s. As we turn on other parameters,
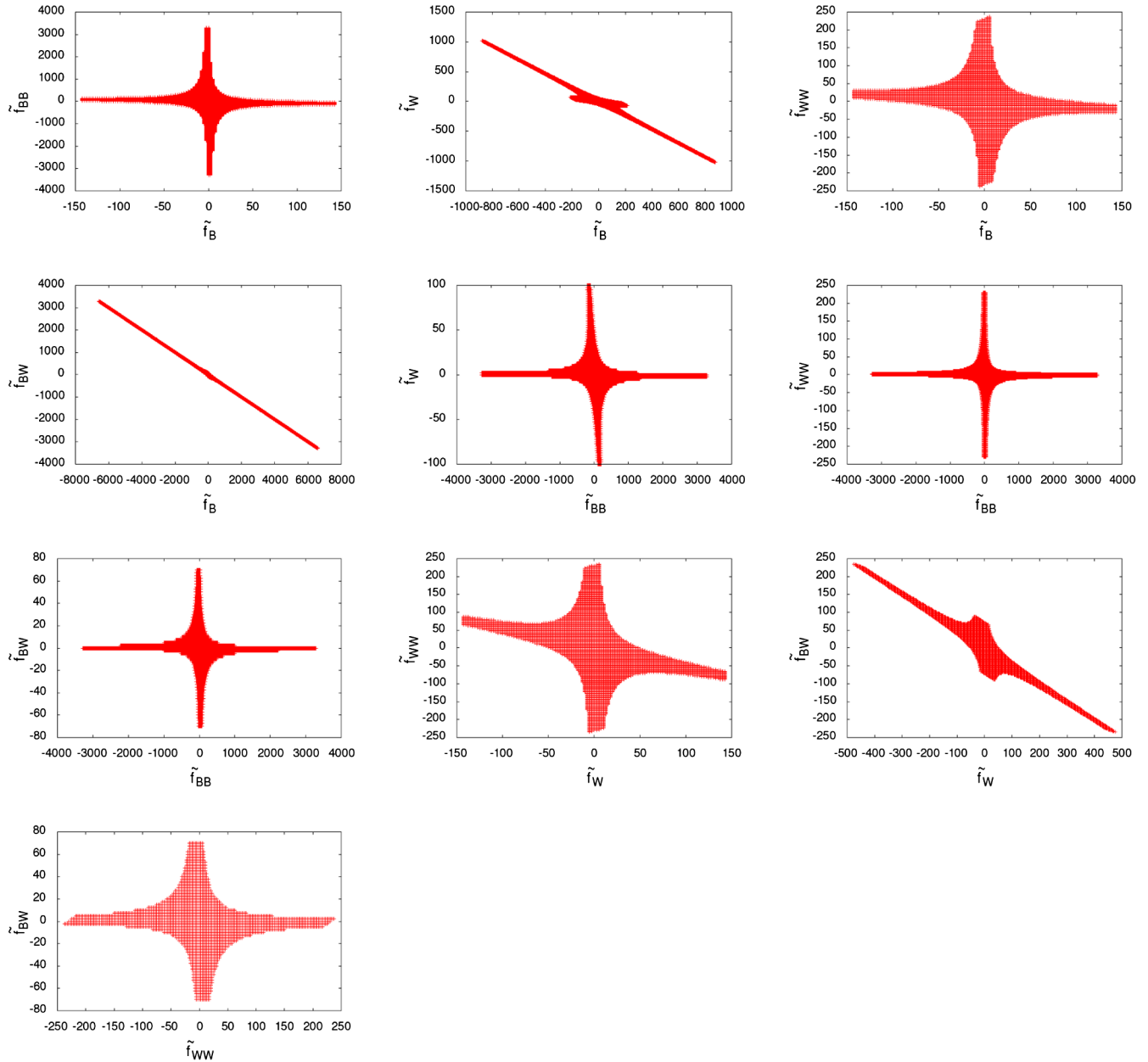
FIG. 2 (color online).   Constraints from electroweak precision data keeping two parameters nonzero at a time and for $\Lambda = 1$ TeV.

these constraints become weaker. Also, for a larger cutoff scale the allowed parameter space grows as one would expect.

IV. CONSTRAINTS FROM LHC DATA

The presence of *CP*-odd operators introduces modifications in the strength of the gauge-Higgs couplings, and hence changes the Higgs production and decay rates in channels involving these couplings. Since we are interested in *CP*-even observables, the SM VVh couplings which are *CP*-even, do not interfere with the *CP*-odd VVh couplings. Hence the lowest order (tree level) modifications to the decay widths (Γ) and production cross sections (σ) are of

the order $\frac{1}{\Lambda^4}$. To quantify these changes we define the following ratios for various decay and production channels,

$$\alpha_Y = \frac{\Gamma^{\mathrm{BSM}}(h \to Y)}{\Gamma^{\mathrm{SM}}(h \to Y)} \qquad (19)$$

$$\gamma_X = \frac{\sigma^{\mathrm{BSM}}(X \to h)}{\sigma^{\mathrm{SM}}(X \to h)} \qquad (20)$$

where Y and X are used to label the final state and initial state particles in the Higgs decay and production channels respectively.

A. Higgs decay channels

In the SM, the 126 GeV Higgs boson predominantly decays into $b\bar{b}$ and WW^* followed by gg, $\tau^+\tau^-$, $c\bar{c}$ and ZZ^*. It also decays to $\gamma\gamma$, γZ and $\mu^+\mu^-$ with much suppressed rates. Out of these, $h \to gg$, $h \to \gamma\gamma$ and $h \to \gamma Z$ are loop-induced decay modes and hence are sensitive to new physics. The decay channels which are affected by the CP-odd operators are $h \to \gamma\gamma$, $h \to \gamma Z$, $h \to WW^*$ and $h \to ZZ^*$. The expressions for the ratio of the decay widths, α_{ij} in various two body Higgs decay channels are as follows[3]:

$$\alpha_{\gamma\gamma} = 1 + 2.84\left(\frac{C_{\gamma\gamma h}^2}{\Lambda^4}\right) \tag{22}$$

$$\alpha_{\gamma Z} = 1 + 0.856\left(\frac{C_{\gamma Z h}^2}{\Lambda^4}\right) \tag{23}$$

$$\alpha_{WW^*} = 1 + 3.35 \times 10^{-6}\left(\frac{C_{WWh}^2}{\Lambda^4}\right) \tag{24}$$

$$\alpha_{2\ell 2\nu} = 1 + 3.56 \times 10^{-6}\left(\frac{C_{WWh}^2}{\Lambda^4}\right) \tag{25}$$

$$\alpha_{ZZ^*} = 1 + 1.40 \times 10^{-6}\left(\frac{C_{ZZh}^2}{\Lambda^4}\right) \tag{26}$$

$$\alpha_{4\ell} = 1 + 1.54 \times 10^{-6}\left(\frac{C_{ZZh}^2}{\Lambda^4}\right) \tag{27}$$

Since the set of gauge-Higgs operators considered in our analysis do not alter the Higgs coupling with gluons (g) and fermions (f), we have $\alpha_{ff} = \alpha_{gg} = 1$. The ratios $\alpha_{2\ell 2\nu}$ [Eq. (25)] and $\alpha_{4\ell}$ [Eq. (27)] correspond to the $h \to WW^* \to 2\ell 2\nu$ and $h \to ZZ^* \to 4\ell$ respectively. Here ℓ stands for electron and muon, and ν for corresponding neutrinos. The ratios α_{WW^*} and α_{ZZ^*} which include both

leptonic and hadronic decays of W and Z bosons are used in calculating modified total Higgs decay width. As mentioned earlier, the modifications to Higgs partial decay widths at leading order are $\mathcal{O}(1/\Lambda^4)$. It is in contrast to the case of CP-even dimension six gauge-Higgs operators where such modifications occur at $\mathcal{O}(1/\Lambda^2)$. Unlike WWh and ZZh couplings, the $\gamma\gamma h$ and γZh couplings are loop-induced in the SM. In the presence of CP-odd operators these vertices receive contributions at tree level. This explains the relatively large coefficients in the expressions for $\alpha_{\gamma\gamma}$ [Eq. (22)] and $\alpha_{\gamma Z}$ [Eq. (23)] as compared to the other decay width ratios. This would imply most stringent constraints on the parameters contributing to these decay channels. For further discussion on CP-odd vs CP-even operators, we refer the reader to Sec. VI.

B. Higgs production channels

At the LHC, the dominant mode to produce Higgs boson is gluon-gluon fusion (GGF) mediated by a top quark loop. The other major production channels include: vector boson fusion (VBF), associated production with a weak boson (Vh) and associated production with a pair of top quark ($t\bar{t}h$). Except GGF and $t\bar{t}h$ production channels, all other channels are affected in presence of anomalous gauge-Higgs CP-odd vertices. Like the decay width ratios, the production cross section ratios also receive modifications at $\mathcal{O}(1/\Lambda^4)$. The ratios of the Higgs production cross sections, γ_X in various channels at $\sqrt{S} = 8(7)$ TeV LHC are given below.

$$\gamma_{pp \to Wh} = 1 + 5.61(5.37) \times 10^{-4}\left(\frac{C_{WWh}^2}{\Lambda^4}\right) \tag{28}$$

$$\gamma_{pp \to Wh \to hl\nu} = 1 + 5.67(5.16) \times 10^{-4}\left(\frac{C_{WWh}^2}{\Lambda^4}\right) \tag{29}$$

$$\gamma_{pp \to Zh} = 1 + 4.09(3.92) \times 10^{-4}\left(\frac{C_{ZZh}^2}{\Lambda^4}\right) + 2.45(2.32) \times 10^{-4}\left(\frac{C_{\gamma Zh}^2}{\Lambda^4}\right)$$
$$+ 2.55(2.44) \times 10^{-4}\left(\frac{C_{ZZh}}{\Lambda^2}\right)\left(\frac{C_{\gamma Zh}}{\Lambda^2}\right) \tag{30}$$

---

[3]We disagree with the CP-odd part of the analytic expression for $\alpha_{\gamma Z}$ in Eq. (3.17) of Ref. [45]. The correct expression for CP-odd term in the notations of Ref. [45] turns out to be,

$$\alpha_{\gamma Z} = 1 + \left|\frac{4\sqrt{2}\pi^2\tilde{a}_2}{G_F\Lambda^2 s_W^2(A_F + A_W)}\right|^2, \tag{21}$$

where $\tilde{a}_2$ can be identified with the factor $\frac{1}{2}C_{\gamma Zh}$ in our notation.

$$\gamma_{\text{VBF}} = 1 + 7.02(5.62) \times 10^{-6}\left(\frac{\tilde{f}_B^2}{\Lambda^4}\right) + 1.50(1.44) \times 10^{-4}\left(\frac{\tilde{f}_W^2}{\Lambda^4}\right) + 1.84(1.80) \times 10^{-5}\left(\frac{\tilde{f}_{BB}^2}{\Lambda^4}\right)$$

$$+ 6.98(6.75) \times 10^{-4}\left(\frac{\tilde{f}_{WW}^2}{\Lambda^4}\right) + 4.39(4.38) \times 10^{-5}\left(\frac{\tilde{f}_{BW}^2}{\Lambda^4}\right) - 1.32(1.14) \times 10^{-5}\left(\frac{\tilde{f}_B\tilde{f}_W}{\Lambda^4}\right)$$

$$+ 8.96(22.2) \times 10^{-7}\left(\frac{\tilde{f}_B\tilde{f}_{BB}}{\Lambda^4}\right) - 5.06(5.03) \times 10^{-5}\left(\frac{\tilde{f}_B\tilde{f}_{WW}}{\Lambda^4}\right)$$

$$+ 2.63(2.59) \times 10^{-5}\left(\frac{\tilde{f}_B\tilde{f}_{BW}}{\Lambda^4}\right) + 8.98(9.21) \times 10^{-7}\left(\frac{\tilde{f}_W\tilde{f}_{BB}}{\Lambda^4}\right)$$

$$+ 6.22(5.98) \times 10^{-4}\left(\frac{\tilde{f}_W\tilde{f}_{WW}}{\Lambda^4}\right) - 2.46(2.71) \times 10^{-5}\left(\frac{\tilde{f}_W\tilde{f}_{BW}}{\Lambda^4}\right)$$

$$- 3.51(3.60) \times 10^{-5}\left(\frac{\tilde{f}_{BB}\tilde{f}_{BW}}{\Lambda^4}\right) + 3.27(3.85) \times 10^{-5}\left(\frac{\tilde{f}_{BB}\tilde{f}_{WW}}{\Lambda^4}\right)$$

$$- 1.43(1.45) \times 10^{-4}\left(\frac{\tilde{f}_{WW}\tilde{f}_{BW}}{\Lambda^4}\right) \tag{31}$$

$$\gamma_{pp\rightarrow tth} = \gamma_{\text{GGF}} = 1. \tag{32}$$

These expressions have been obtained by computing the SM and BSM cross sections at tree level using MADGRAPH [61] under the assumption that the K-factors (due to higher order corrections) are same in the SM and BSM cases. For that we have implemented our effective Lagrangian in FEYNRULES [62] and used the generated UFO model file in MADGRAPH. The cross sections have been calculated using CTEQ6L1 parton distribution functions [63] and with default settings for renormalization and factorization scales.

We would like to point out that there is an additional diagram which contributes to $pp \rightarrow Zh$ due to tree level *CP*-odd γZh coupling. Similarly, in VBF channel additional diagrams appear due to both $\gamma\gamma h$ and γZh couplings. Because of a different parametrization, this information is not explicit in the expression for VBF. We find this parametrization more convenient in terms of evaluating the coefficients in Eq. (31). Also, the VBF coefficients reported above do not have any Vh contamination and this can be ensured in MADGRAPH at the process generation level. One can notice that the modifications induced by the *CP*-odd operators are relatively weak because the SM cross sections are already tree level effects in the modified production channels.

One important fact in relation to these production cross section ratios (γs) is that the numerical coefficients present in these expressions are very much cut dependent. This is associated with the fact that the anomalous couplings induced by the gauge-Higgs operators have a different Lorentz structure (therefore, different kinematic dependence) than their SM counterparts. Hence in general the SM and BSM cut efficiencies are not the same for a given process. The differences between the two become more pronounced for higher values of the *CP*-odd couplings. But

for reasonably low values of the same one can still work under the approximation that the two cut efficiencies are the same. In this work we have taken this approximation into consideration, and taken only default cuts in MADGRAPH to simulate any production or decay channel. Since we have taken data only from individual production channels and not from combined channel data (e.g. Vh combined channel) in our chi-square analysis, this approximation finds a stronger footing.

C. Global analysis

The quantitative measure of the difference between the Higgs data from the LHC, and its corresponding SM predictions is given by what we call the signal strength, defined as,

$$\mu^{X,Y} = \frac{\sigma^{\text{BSM}}(X \rightarrow h)\text{BR}^{\text{BSM}}(h \rightarrow Y)}{\sigma^{\text{SM}}(X \rightarrow h)\text{BR}^{\text{SM}}(h \rightarrow Y)} \tag{33}$$

where, $\text{BR}(h \rightarrow Y) = \frac{\Gamma(h \rightarrow Y)}{\Gamma_{\text{total}}}$ is the branching ratio for Higgs decaying into Y final state, and Γ_{total} is the total Higgs decay width. For 126 GeV Higgs boson $\Gamma_{\text{total}}^{\text{SM}} = 4.2$ MeV. The total Higgs decay width in the BSM construct $\Gamma_{\text{total}}^{\text{BSM}}$ can be expressed in terms of the SM total Higgs decay width $\Gamma_{\text{total}}^{\text{SM}}$ by,

$$\Gamma_{\text{total}}^{\text{BSM}} = S_{\text{total}}\Gamma_{\text{total}}^{\text{SM}}. \tag{34}$$

S_{total} is given in terms of the various branching fractions of the Higgs in the SM as,

$$S_{\text{total}} \sim \text{BR}_{bb}^{\text{SM}} + \text{BR}_{cc}^{\text{SM}} + \text{BR}_{\tau\tau}^{\text{SM}} + \alpha_{\gamma\gamma}\text{BR}_{\gamma\gamma}^{\text{SM}} + \alpha_{\gamma Z}\text{BR}_{\gamma Z}^{\text{SM}}$$
$$+ \alpha_{WW^*}\text{BR}_{WW^*}^{\text{SM}} + \alpha_{ZZ^*}\text{BR}_{ZZ^*}^{\text{SM}} + \alpha_{gg}\text{BR}_{gg}^{\text{SM}} \tag{35}$$

TABLE II. Higgs production cross section in the SM [64].

Production channel	8 TeV cross section (pb)	7 TeV cross section (pb)
GGF	18.97	14.89
VBF	1.568	1.211
Wh	0.686	0.563
Zh	0.405	0.327
$t\bar{t}h$	0.1262	0.0843
$b\bar{b}h$	0.198	0.152

which becomes on solving,

$$S_{\text{total}} \sim 0.736 + 0.0023\alpha_{\gamma\gamma} + 0.0016\alpha_{\gamma Z}$$
$$+ 0.23\alpha_{WW^*} + 0.029\alpha_{ZZ^*}. \qquad (36)$$

The SM branching fractions for 126 GeV Higgs are taken from [64]. The signal strength in Eq. (33) can be rewritten in a compact form using the decay and the productions cross section ratios defined above,

$$\mu^{X,Y} = \gamma_X \frac{\alpha_Y}{S_{\text{total}}}. \qquad (37)$$

To perform the global fit of our *CP*-odd parameters, we use the standard definition of the chi-square function,

$$\chi^2 = \sum_{X,Y} \frac{(\mu_{th}^{X,Y} - \mu_{\exp}^{X,Y})^2}{\Sigma_{X,Y}^2} \qquad (38)$$

where $\mu_{th}^{X,Y}$ is the theoretical signal strength expected in presence of *CP*-odd operators, and $\mu_{\exp}^{X,Y}$ is the experimental signal strength reported by the LHC experiments. $\Sigma_{X,Y}$ is the experimental uncertainty in $\mu_{\exp}^{X,Y}$. The experimental data reported generally has unsymmetrical uncertainties $\Sigma_{X,Y}^+$ and $\Sigma_{X,Y}^-$. The $\Sigma_{X,Y}$ that we use symmetrizes these uncertainties through the following definition,

$$\Sigma_{X,Y} = \sqrt{\frac{(\Sigma_{X,Y}^+)^2 + (\Sigma_{X,Y}^-)^2}{2}}. \qquad (39)$$

Since the LHC data that we use includes data from both 7 and 8 TeV LHC runs, the theoretical signal strength in Eq. (38) is obtained after combining the signal strengths calculated for 7 and 8 TeV LHC. For that we have used following formula [43],

$$\mu_{th}^{XY} = \frac{\mu_{th,8}^{XY}\sigma_8^{\text{SM}}\mathcal{L}_8 + \mu_{th,7}^{XY}\sigma_7^{\text{SM}}\mathcal{L}_7}{\sigma_8^{\text{SM}}\mathcal{L}_8 + \sigma_7^{\text{SM}}\mathcal{L}_7} \qquad (40)$$

where $\mathcal{L}_7$ and $\mathcal{L}_8$ are the luminosities at 7 and 8 TeV, respectively, and σ_7^{SM} and σ_8^{SM} are the SM cross sections at those energies. These cross sections are listed in Table II.

In our analysis we have taken total 15 data points which are the most updated ones. We have listed them in Table III. Note that due to large uncertainty we do not include Higgs data in $h \rightarrow \gamma Z$ decay channel [65,66] from CMS and ATLAS. The global analysis with five *CP*-odd parameters results into $\chi^2_{\text{min}} = 6.78$. However, in this case the best fit point is very unstable with respect to the step size that we

TABLE III. LHC data used in the global analysis.

Production channel	Decay channel	Signal strength	Energy in TeV (Luminosity in fb^{-1})
GGF (ATLAS)	$h \rightarrow \gamma\gamma$	1.32 ± 0.38 [67]	$7(4.5) + 8(20.3)$
VBF (ATLAS)	$h \rightarrow \gamma\gamma$	0.8 ± 0.7 [67]	$7(4.5) + 8(20.3)$
Wh (ATLAS)	$h \rightarrow \gamma\gamma$	1.0 ± 1.6 [67]	$7(4.5) + 8(20.3)$
Zh (ATLAS)	$h \rightarrow \gamma\gamma$	$0.1^{+3.7}_{-0.1}$ [67]	$7(4.5) + 8(20.3)$
$t\bar{t}h$ (ATLAS)	$h \rightarrow \gamma\gamma$	$1.6^{+2.7}_{-1.8}$ [67]	$7(4.5) + 8(20.3)$
GGF (CMS)	$h \rightarrow \gamma\gamma$	$1.12^{+0.37}_{-0.32}$ [68]	$7(5.1) + 8(19.7)$
VBF (CMS)	$h \rightarrow \gamma\gamma$	$1.58^{+0.77}_{-0.68}$ [68]	$7(5.1) + 8(19.7)$
$t\bar{t}h$ (CMS)	$h \rightarrow \gamma\gamma$	$2.69^{+2.51}_{-1.81}$ [68]	$7(5.1) + 8(19.7)$
GGF + $t\bar{t}h$ + $b\bar{b}h$ (ATLAS)	$h \rightarrow ZZ^* \rightarrow 4\ell$	$1.7^{+0.5}_{-0.4}$ [69]	$7(4.5) + 8(20.3)$
GGF + $t\bar{t}h$ (CMS)	$h \rightarrow ZZ^* \rightarrow 4\ell$	$0.8^{+0.46}_{-0.36}$ [70]	$7(5.1) + 8(19.7)$
GGF (ATLAS)	$h \rightarrow WW^* \rightarrow 2\ell2\nu$	$1.01^{+0.27}_{-0.25}$ [71]	$7(4.5) + 8(20.3)$
VBF (ATLAS)	$h \rightarrow WW^* \rightarrow 2\ell2\nu$	$1.28^{+0.53}_{-0.45}$ [71]	$7(4.5) + 8(20.3)$
GGF (CMS)	$h \rightarrow WW^* \rightarrow 2\ell2\nu$	$0.74^{+0.22}_{-0.20}$ [72]	$7(4.9) + 8(19.4)$
VBF (CMS)	$h \rightarrow WW^* \rightarrow 2\ell2\nu$	$0.6^{+0.57}_{-0.46}$ [72]	$7(4.9) + 8(19.4)$
$Wh \rightarrow h\ell\nu$ (CMS)	$h \rightarrow WW^* \rightarrow 2\ell2\nu$	$0.56^{+1.27}_{-0.95}$ [72]	$7(4.9) + 8(19.4)$

choose to scan the parameter space. Also, we find that the $\chi^2_{\min}$ is insensitive to the parameters $\tilde{f}_B$ and $\tilde{f}_W$. These are the parameters which do not enter the $\gamma\gamma h$ vertex and their coefficients are very small compared to those of $\tilde{f}_{BB}$, $\tilde{f}_{WW}$ and $\tilde{f}_{BW}$, which do enter the $\gamma\gamma h$ vertex [Eq. (22)]. Since the LHC observables have an overall cutoff scale dependence, the ratio $\tilde{f}_i/\Lambda^2$ can be taken as the effective parameter to be constrained. In other words, the constraints from global analysis can be easily predicted for any value of Λ of interest.

We organize the constraints on *CP*-odd parameters from global fit of LHC data in the following two parts.

 (i) We have five *CP*-odd parameters ($\tilde{f}_W$, $\tilde{f}_B$, $\tilde{f}_{BB}$, $\tilde{f}_{BW}$, $\tilde{f}_{WW}$) and in the first case we consider any two of them to be non-zero and put limits on them. There are a total of ten such combinations. The allowed parameter space with 68% and 95% confidence levels are shown in Fig. 3. In generating these plots we have varied parameters freely. Even if one considers the perturbativity argument, the tightest upper bound on these *CP*-odd parameters is of the order ∼100. We can see that in all cases the allowed parameter space is bounded. The parameters which enter the $\gamma\gamma h$ vertex ($\gamma\gamma h$ family) i.e., $\tilde{f}_{BB}$, $\tilde{f}_{WW}$ and $\tilde{f}_{BW}$ are in general more constrained than those which do not enter the $\gamma\gamma h$ vertex (non-$\gamma\gamma h$ family) i.e., $\tilde{f}_B$ and $\tilde{f}_W$. When any of the three $\gamma\gamma h$ parameters is taken together with $\tilde{f}_B$ or $\tilde{f}_W$ as shown in Figs. 3(a),3(c)–3(e),3(h) and 3(i), we find that it is much tightly constrained and allowed values are of $\mathcal{O}(1)$. However, among themselves these parameters are highly correlated and cancellation among them leads to larger allowed values of $\mathcal{O}(10)$ [see Figs. 3(f),3(g) and 3(j)]. The nature of slope in these figures is related to the relative sign among $\tilde{f}_{BB}$, $\tilde{f}_{WW}$ and $\tilde{f}_{BW}$. We also note that out of $\tilde{f}_B$ and $\tilde{f}_W$, $\tilde{f}_W$ is always more constrained. For example, the maximum allowed value for $\tilde{f}_B$ is ∼100 while the allowed values of $\tilde{f}_W$ are less than 60, see Fig. 3(b). This observation can be attributed to the relative size of their coefficients in various observables. We have also found that the inclination of the plot in Fig. 3(b) is governed by the $C_{\gamma Zh}$ which enters Zh and VBF production channels and affects the S_{total} [Eq. (36)].

 (ii) In the second case we consider three parameters at a time in the global analyses. Once again there are ten such combinations. Following the general conclusions of two-parameter case, we can categorize these combinations into three groups. This categorization is based on the number of parameters from the $\gamma\gamma h$ family being present in each combination. Thus we have one combination where all the parameters are from $\gamma\gamma h$ family (G1), six combinations where two parameters are from $\gamma\gamma h$ family and one from non-$\gamma\gamma h$ family (G2) and three combinations where one is from $\gamma\gamma h$ family and the other two are $\tilde{f}_B$ and $\tilde{f}_W$ (G3). We present results for three representative combinations (one from each group): (i) $\{\tilde{f}_{BB}, \tilde{f}_{WW}, \tilde{f}_{BW}\}$; (ii) $\{\tilde{f}_{BB}, \tilde{f}_{WW}, \tilde{f}_B\}$; (iii) $\{\tilde{f}_{WW}, \tilde{f}_B, \tilde{f}_W\}$. The allowed parameter space for these combinations are shown in Figs. 4, 5 and 6, respectively. The two-parameter plots here are obtained after marginalizing over the third parameter.

As compared to two-parameter plots (see Fig. 3), the allowed region here is more diffused due to the presence of the third parameter. This is particularly noticeable for the first set of plots in Fig. 4. We find that $\tilde{f}_{WW}$ being present in all VVh couplings gets stronger bounds, while $\tilde{f}_{BW}$ is least constrained in set (i). From the plots of Fig. 5 which belong to set (ii) we can infer that the parameters of $\gamma\gamma h$ family are more constrained. However, mutual cancellation still allows values of $\mathcal{O}(30)$ for them. The opposite inclinations of the plots in Figs. 5(a) and 5(b) can be related to how $\tilde{f}_{BB}$ and $\tilde{f}_{WW}$ enter in $\gamma\gamma h$ vertex to maintain cancellation and it is confirmed by the nature of the slope in Fig. 5(c). Note that Fig. 5(c) is very much similar to the corresponding plot in Fig. 3(f). This is expected because the global analysis is not very sensitive to $\tilde{f}_B$. Interestingly, the parameter sets $\{\tilde{f}_{WW}, \tilde{f}_{BW}, \tilde{f}_W\}$ and $\{\tilde{f}_{BB}, \tilde{f}_{BW}, \tilde{f}_B\}$ which would also belong to group G2 are less constrained. We find that the parameter regions are still bounded but boundary values for $\tilde{f}_W$ and $\tilde{f}_B$ in these sets are about 800 and 2500, respectively. For the parameters in set (iii) we can conclude that $\tilde{f}_{WW}$ being the only parameter present from the $\gamma\gamma h$ family is very tightly constrained as shown by the plots in Figs. 6(b) and 6(c).

We have also checked that the constraints on *CP*-odd parameters from the direct and indirect measurements of the Higgs total width [70,73] are weaker than those obtained from the global analysis. On the whole, $\tilde{f}_{BB}$, $\tilde{f}_{WW}$ and $\tilde{f}_{BW}$ contribute to the $\gamma\gamma h$ vertex at tree level and thus are constrained rather tightly compared to $\tilde{f}_B$ and $\tilde{f}_W$. The fact that one has SM contribution at the one-loop level only is responsible for this. $\tilde{f}_B$ and $\tilde{f}_W$ are relatively loosely constrained due to the lack of sufficient data on the channel $h \to \gamma Z$, to which they contribute.

The constraints on the parameter space of our *CP*-violating operators, as obtained from global fits of the $(7 + 8)$ TeV data, are expected to be improved in the high energy runs. A tentative estimate of such improvements, as also that in a linear e^+e^- collider, can be found, for example, in [74]. Going by the estimates of [74], the uncertainty in the signal strength measurements in the
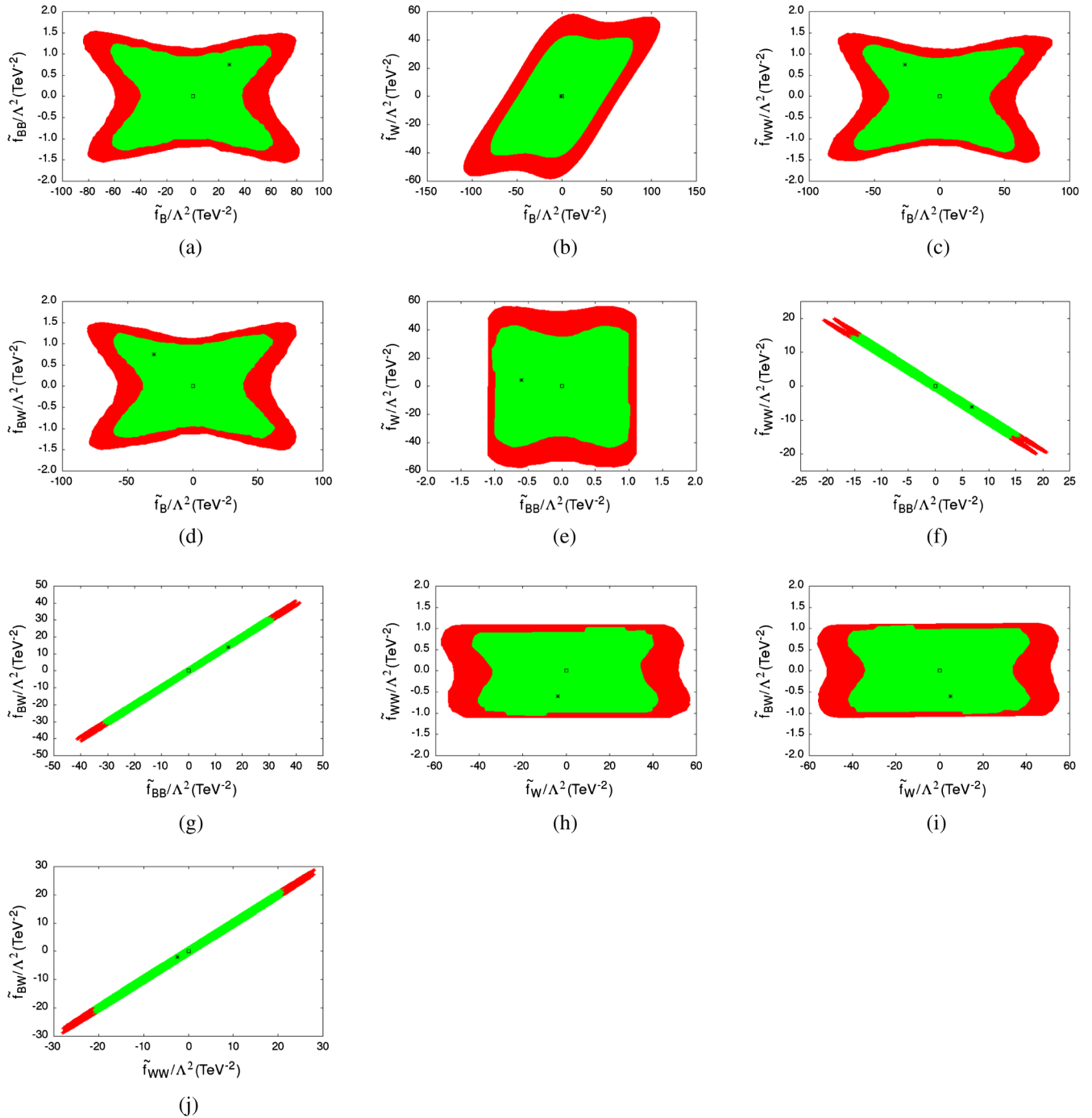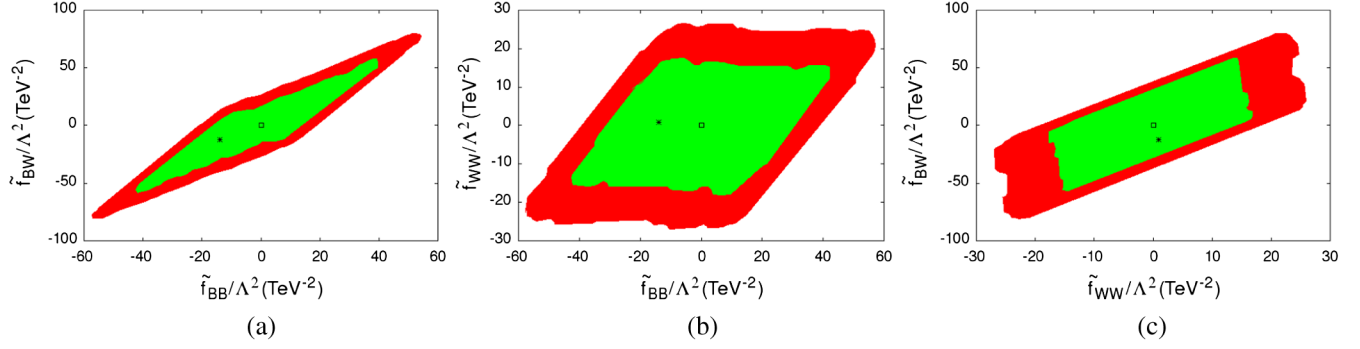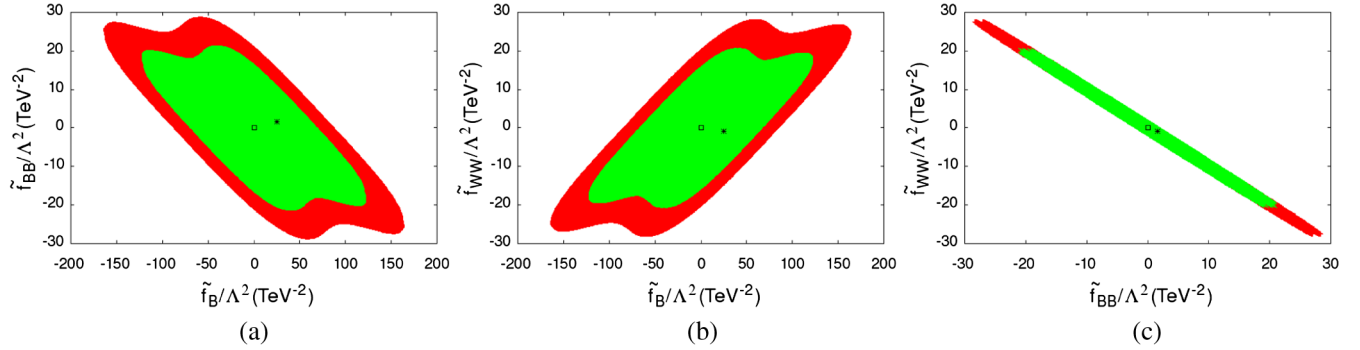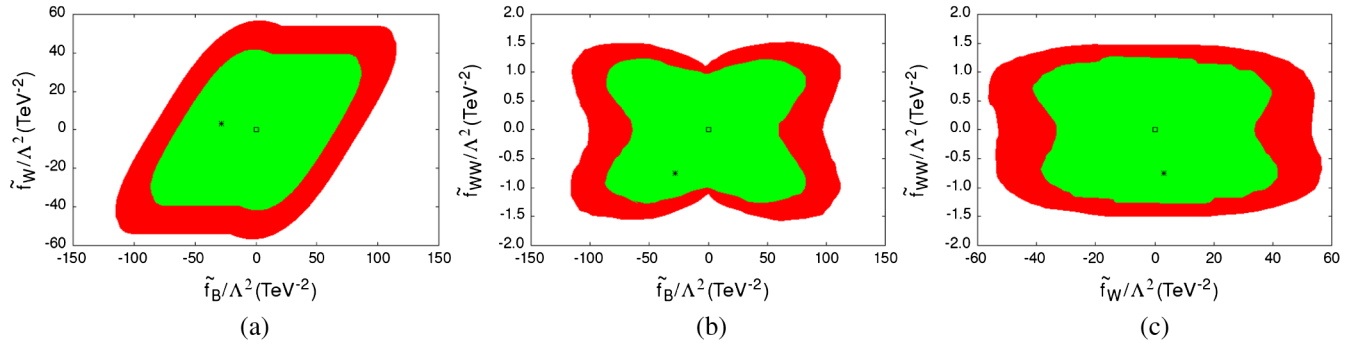
FIG. 3 (color online).   Global fits of the *CP*-odd parameters keeping two parameters nonzero at a time. The point (0, 0) corresponds to the SM point and the (asterisk) represents the best fit point. The green region corresponds to the 68 percent confidence interval and the red region to the 95 percent confidence interval, respectively. The best fit point is doubly degenerate up to a sign flip of the best fit point coordinates.

next run can be reduced to 33% of the present uncertainties as obtained by both ATLAS and CMS for the $\gamma\gamma$ and WW^* final states in the gluon fusion channel. A precise answer on the improvement of our limits, however, depends also on any possible shift in the central values of the measured signal strengths in different channels. This in turn is also a function of the various systematic uncertainties in

the new run, and therefore we have to wait for more data before some precise conclusions can be drawn. A similar consideration applies to a linear collider; precision in coupling measurements down to 1% is expected there in principle [74], but the available statistics as well as the systematics need to be known before concrete estimates emerge.

FIG. 4 (color online).   Marginalized global fits of the *CP*-odd parameters with $\tilde{f}_W = \tilde{f}_B = 0$.

FIG. 5 (color online).   Marginalized global fits of the *CP*-odd parameters with $\tilde{f}_W = \tilde{f}_{BW} = 0$.

FIG. 6 (color online).   Marginalized global fits of the *CP*-odd parameters with $\tilde{f}_{BB} = \tilde{f}_{BW} = 0$.

V. CONSTRAINTS FROM EDMS

The fermionic electric dipole moment receive an additional contribution from these new *CP*-odd higher-dimensional operators involving Higgs and pair of gauge bosons. Nonobservation of any fermionic EDMs puts severe constraints on the parameters $\tilde{f}_i$s. The fermion EDM operator is defined as,

$$-\frac{1}{2} d_f \bar{\psi}(p_2) i\gamma^5 \sigma^{\mu\nu} \psi(p_1) F_{\mu\nu}, \qquad (41)$$

where, $\sigma^{\mu\nu} = \frac{i}{2}[\gamma^\mu, \gamma^\nu]$ and d_f is known as the fermion EDM form factor. Nonvanishing EDMs provide clear hint of

CP-violation [75,76]. In the standard model, *CP* violation occurs due to quark mixing and it is quite weak (1 part in 1000) [50]. On top of that the first nonzero contribution to EDM operator in the SM appears at three loop level in quark sector, while, for leptons it arises at four loop level. The present upper limits on electron and neutron EDMs are much larger than the values predicted by the SM [77]. In presence of *CP*-odd gauge-Higgs operators $\gamma\gamma h$, γZh and $WW\gamma$ couplings are modified, because of which the leading contribution to fermion EDMs appears at one-loop level. Due to this the fermion EDM measurements can provide stringent bounds on the *CP*-odd parameters. Note that the contribution to the fermion EDMs from *CP*-odd WWh and
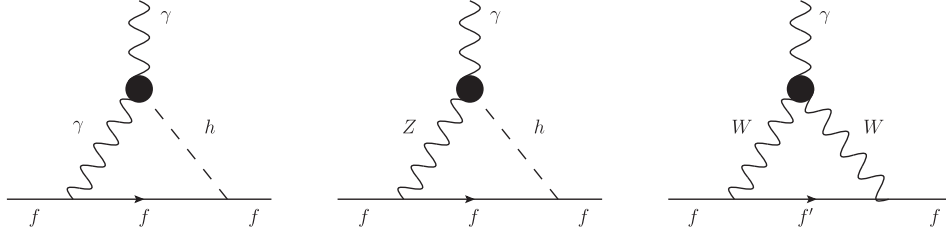
FIG. 7.   One-loop diagrams contributing to fermion EDMs. The blobs show the effective vertices arising out of the *CP*-odd operators.

ZZh vertices can result only at two-loop level. Since the two-loop effects are expected to be subdominant, we will derive constraints on the *CP*-odd parameters from one-loop fermion EDM calculations. The diagrams that contribute to the fermion EDM at one-loop level are shown in Fig. 7.

The expression for the fermion EDM form factor d_f at one-loop due to the $\gamma\gamma h$, γZh and $WW\gamma$ vertices is given by the following equation[4]:

$$d_f = \frac{m_f e\alpha}{\pi v^2} [\tilde{a}_1 K_1(\Lambda, m_h) + \tilde{a}_2 K_2(\Lambda, m_Z, m_h)$$
$$+ \tilde{a}_3 K_1(\Lambda, m_W)] \tag{42}$$

where,

$$\tilde{a}_1 = -\frac{Q_f}{4s_W^2} C_{\gamma\gamma h}; \quad \tilde{a}_2 = \frac{(\frac{1}{2}I_f - Q_f s_W^2)}{t_W s_{2W}^2} C_{\gamma Zh};$$

$$\tilde{a}_3 = -\frac{I_f}{4s_W^3} C_{WW\gamma}. \tag{43}$$

Here, v is the electroweak symmetry breaking scale, α is the fine structure constant, I_f is the third component of the fermion Isospin and Q_f is its electric charge quantum number. We have neglected the fermion masses (m_f) with respect to other mass scales in the loop. The one-loop factors K_1 and K_2 are calculated in dimensional regularization ($d = 4 - 2\epsilon$). Since these loops are UV divergent, we renormalize them in $\overline{\text{MS}}$ scheme and identify the renormalization scale with the cutoff Λ. The expressions for K_1 and K_2 are given by,

$$K_1(\Lambda, x) = \frac{v^2}{\Lambda^2} \left[\frac{1}{2}\ln\frac{\Lambda^2}{x^2} + \frac{3}{4}\right], \tag{44}$$

$$K_2(\Lambda, x, y) = \frac{v^2}{\Lambda^2} \left[\frac{1}{2}\frac{x^2 \ln\frac{\Lambda^2}{x^2} - y^2 \ln\frac{\Lambda^2}{y^2}}{x^2 - y^2} + \frac{3}{4}\right]. \tag{45}$$

In the above, the finite factors of $\frac{3}{4}$ are artifact of dimensional regularization. These factors do not appear in naive cutoff regularization.

_____
[4]We have observed a relative sign change in the contribution of the $WW\gamma$ diagram to the EDM, for the u and d quarks, which is taken care of by the factor I_f in $\tilde{a}_3$. It was unaccounted by Ref. [45] where a similar calculation is done.

The latest experimental bounds on the electron and neutron EDMs are [78–80],

$$|d_e| < 8.7 \times 10^{-29} \ e \ \text{cm}$$
$$|d_n| < 2.9 \times 10^{-26} \ e \ \text{cm}. \tag{46}$$

Note that the EDM contribution is $\mathcal{O}(\frac{1}{\Lambda^2})$ in the cutoff scale, therefore, it is expected to provide stronger bounds on *CP*-odd parameters than those obtained from EWP and LHC data. Like the electroweak precision observables calculated in Sec. III, the EDMs also have explicit dependence on Λ. Due to this, we provide EDM constraint equations for three different choices of cutoff scale $\Lambda = 1$, 5 and 10 TeV.
   (i) $\Lambda = 1$ TeV

$$|d_e| \equiv |233.86\tilde{f}_B + 260.45\tilde{f}_W - 390.92\tilde{f}_{BB}$$
$$- 337.72\tilde{f}_{WW} + 858.63\tilde{f}_{BW}| < 1$$
$$|d_n| \equiv |7.02\tilde{f}_B + 13.81\tilde{f}_W - 8.91\tilde{f}_{BB}$$
$$+ 4.66\tilde{f}_{WW} + 22.96\tilde{f}_{BW}| < 1 \tag{47}$$

   (ii) $\Lambda = 5$ TeV

$$|d_e| \equiv |13.87\tilde{f}_B + 15.63\tilde{f}_W - 24.60\tilde{f}_{BB}$$
$$- 21.08\tilde{f}_{WW} + 52.34\tilde{f}_{BW}| < 1$$
$$|d_n| \equiv |0.40\tilde{f}_B + 0.85\tilde{f}_W - 0.57\tilde{f}_{BB}$$
$$+ 0.33\tilde{f}_{WW} + 1.36\tilde{f}_{BW}| < 1 \tag{48}$$

   (iii) $\Lambda = 10$ TeV

$$|d_e| \equiv |3.95\tilde{f}_B + 4.47\tilde{f}_W - 7.11\tilde{f}_{BB}$$
$$- 6.08\tilde{f}_{WW} + 15.02\tilde{f}_{BW}| < 1$$
$$|d_n| \equiv |0.11\tilde{f}_B + 0.24\tilde{f}_W - 0.16\tilde{f}_{BB}$$
$$+ 0.10\tilde{f}_{WW} + 0.39\tilde{f}_{BW}| < 1 \tag{49}$$

The neutron EDM form factor (d_n) is calculated in terms of constituent quark EDMs using the relation $d_n = \frac{4}{3}d_d - \frac{1}{3}d_u$, from the chiral-quark model [81]. In

calculating the above constraints on the EDMs we take $\alpha = 1/137$ and $M_H = 126$ GeV. Because of a stronger experimental limit on electron EDM, the coefficients of parameters in d_e are larger than those in d_n. Our constraint equations for electron EDM form factor differ by an order of magnitude from those obtained in Ref. [45] mainly because we have used the most updated experimental bound on electron EDM [78].

We first consider the case when any two of the five parameters are kept nonzero. In this case, we freely vary the parameters. The constraints on the parameters are shown in Fig. 8 for $\Lambda = 1$, 5 and 10 TeV respectively. In all combinations we get bounded regions. The inclinations of the constraint regions can be understood from the relative

sign between the parameters in the expressions for the EDMs. As expected the constraints for $\Lambda = 1$ TeV are tighter than those for $\Lambda = 5$ and 10 TeV and this is corroborated by the size of the coefficients entering in EDM expressions. In $\Lambda = 1$ TeV case, the allowed values for parameters can reach $\mathcal{O}(1)$ values at maximum. As we push the cutoff scale higher, the allowed range for parameters also increases. For example, for $\Lambda = 10$ TeV the allowed values can become $\mathcal{O}(10)$ or larger in some cases.

A naive comparison with the EDM calculation carried out in Ref. [49] with only $\gamma\gamma h$ *CP*-odd coupling suggests that for $\Lambda = 1$ TeV, the constraint equation for electron EDM measurement would be $|\tilde{f}_{BB} + \tilde{f}_{WW}| \lesssim 0.0036$. In the presence of *CP*-odd $\gamma Z h$ coupling, which arises from
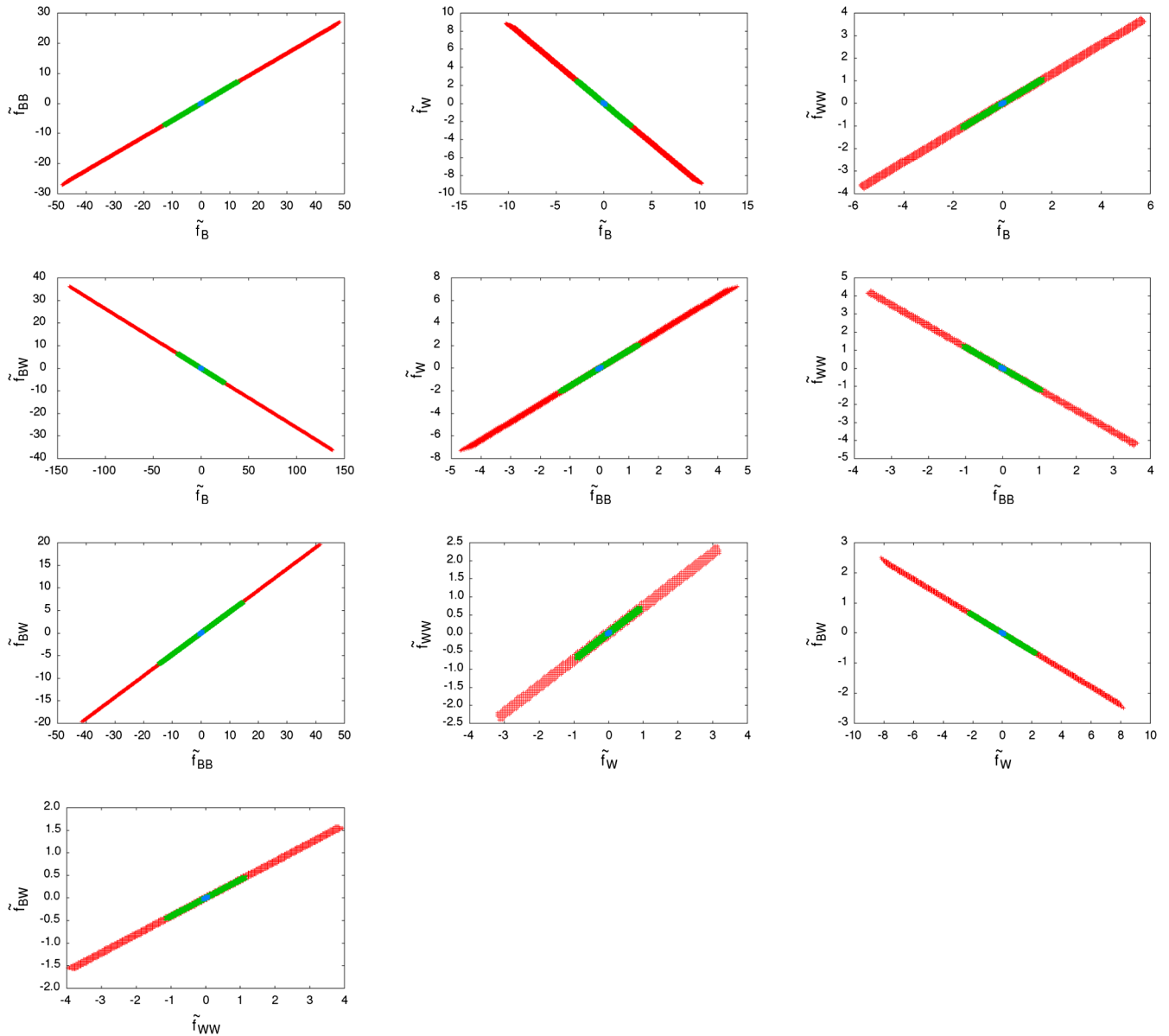

FIG. 8 (color online). EDM constraints keeping two parameters nonzero at a time for three representative values of $\Lambda = 1$ (blue), 5 (green) & 10(red) TeV.

same operators, this constraint equation would change. For example, our calculation for electron EDM constraint implies, $|\tilde{f}_{BB} + 0.86\tilde{f}_{WW}| \lesssim 0.0026$. In both the cases, the parameters would be allowed to take very large but fine-tuned values. However, we would like to point out that after including the constraints from the neutron EDM measurement, these parameters cannot take values larger than $\mathcal{O}(0.1)$.

When we take three parameters nonzero at a time, the parameters are scanned in the range -200 to 200. In Fig. 9, we give two dimensional projection plots of the three dimensional constraint region for $\Lambda = 1$ TeV. For comparison purpose, we present the plots in three categories discussed in the global analysis. We can see that with three parameters present, the constraints are more relaxed than when only two of them are nonzero. However, the parameters are still quite correlated. $\tilde{f}_B$ and $\tilde{f}_{BB}$ can often reach the boundary of the scanned regions. In fact it is very

difficult to obtain closed boundaries. As we increase the range for parameter scan the allowed values for *CP*-odd parameters become very large [$\mathcal{O}(1000)$]. However, it is important to note that for too large values of parameters, the two-loop EDM constraints may become relevant and, therefore, should also be taken into account. As we turn on more parameters, the correlation among parameters constrained by EDM is relaxed and the allowed parameter space also expands.

From the experimental perspective, a number of new EDM experiments promise to improve the level of sensitivity by one to two orders of magnitude in the coming years. For example, The Institut Laue Langevin (ILL) cryogenic experiment and the Spallation Neutron Source (SNS) nEDM experiment ([82,83,84]) aim at improving the upper limit on neutron EDM by two orders of magnitude, i.e. down to $\mathcal{O}(10^{-28})e$.cm. This would imply that the numerical coefficients in the constraint equations for d_n in
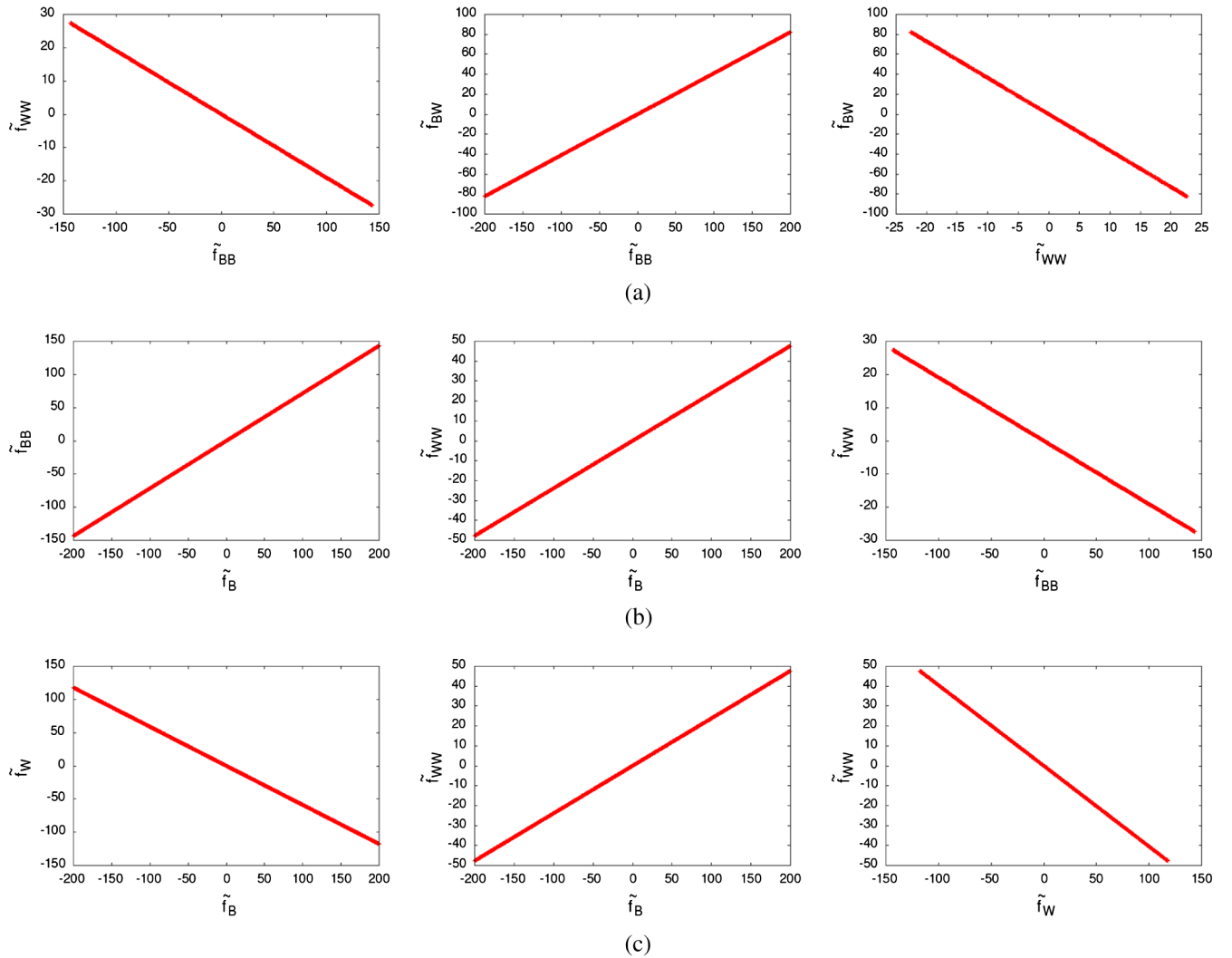

FIG. 9 (color online).   EDM constraints with (a) $\tilde{f}_W = \tilde{f}_B = 0$, (b) $\tilde{f}_W = \tilde{f}_{BW} = 0$ and (c) $\tilde{f}_{BB} = \tilde{f}_{BW} = 0$ for $\Lambda = 1$ TeV. Parameters are varied in the range between -200 to 200.

Eqs. (47), (48) and (49) would become stronger by almost two orders of magnitude and thus the allowed parameter space for $\tilde{f}'$s will be even more severely constrained, unless, of course, there is direct evidence of neutron EDM in the aforesaid experiments.

VI. DISCUSSION

We now highlight the important features of our analysis presented in Secs. III, IV, and V. We try to draw a comparative picture and address some of the issues relevant to the analysis.

(i) In the two parameter case, among all the constraints, the EWP constraints on *CP*-odd parameters are always the weakest while EDM constraints are the strongest. In general, the correlation among parameters is stronger in EWP and EDM cases as compared to the LHC case.

(ii) In case of global fit of LHC data whatever contributes to $h \to \gamma\gamma$ receives stronger constraints, since here the "tree level" contributions from the dimension six operators are essentially at the same level as the "one-loop" SM contributions. There are three such parameters namely $\tilde{f}_{BB}$, $\tilde{f}_{WW}$ and $\tilde{f}_{BW}$. Only a strong cancellation or correlation can keep the individual values of these parameters large.

(iii) The same should apply to parameters contributing to $h \to \gamma Z$ channel which also includes $\tilde{f}_B$ and $\tilde{f}_W$. However the limits based on current data are rather weak there and we have not included them in our analysis. The global analysis puts some limits on $\tilde{f}_B$ and $\tilde{f}_W$ as the γZh coupling modifies the Zh and VBF production channels and the total Higgs decay width.

(iv) The channels dependent on the WWh and ZZh couplings yield relatively weak constraints from the global fits as a whole, since the higher dimensional interactions are inadequate to override the tree level SM contributions.

(v) In two parameter case, LHC data bounds on $\tilde{f}_{BB}$, $\tilde{f}_{BW}$ and $\tilde{f}_{WW}$ are stronger when any of these is combined with $\tilde{f}_B$ or $\tilde{f}_W$. These bounds are comparable to corresponding bounds obtained from EDM measurements.

(vi) In three parameter case, the bounds from LHC data are stronger than those obtained from EDMs. In fact, for some parameters (for example, $\tilde{f}_B$) values of the order 1000 are also allowed by EDM data. However, the parameters constrained from EDMs still display a tight correlation.

(vii) If we allow dimension-6 *CP*-even operators to coexist with the *CP*-odd ones, the EWP and LHC observables would receive contributions at $\mathcal{O}(1/\Lambda^2)$ (as a result of interference with the SM) as well as at $\mathcal{O}(1/\Lambda^4)$. Since there is no interference between *CP*-odd and *CP*-even operators in total rates, the *CP*-odd interactions studied by us should contribute to signal strengths on the order of $(1/\Lambda^4)$. For the sake of consistency, at $\mathcal{O}(1/\Lambda^4)$ the contribution from dimension-8 *CP*-even operators via its interference with the SM should also be considered. Thus, in the presence of *CP*-even operators, the constraints from LHC and precision data can be relaxed. However, under the assumption that the effect of *CP*-conserving new physics is not significantly large, the constraints obtained by us on *CP*-odd operators are in a way the most conservative estimates of the allowed parameter space. Of course, the limits from EDM analyses remain the same in all the cases.

(viii) A comparison between the relative strengths of the EDM and LHC constraints, we emphasize, is most transparent only when the *CP*-violating operators alone are considered, since the *CP*-conserving ones have no role in EDMs. Their inclusion, albeit via marginalization in the LHC global fits, will serve to relax the corresponding limits beyond what we have obtained. But then, it ceases to be a one-to-one comparison between the two kinds of constraints, something that we have intended to do from the beginning.

We have already seen that the Lorentz structure of anomalous *CP*-odd couplings is unique and these are just some linear combinations of the *CP*-odd parameters (see Table I). Since in all the observables these couplings enter directly, it is instructive to know the kind of values these couplings can take as a result of our analysis presented above. In the calculation of S, T and U parameters all the *CP*-odd couplings directly enter. In the global analysis only C_{VVh} couplings participate, therefore, constraints on C_{WWV} from the LHC data are indirect. In EDM calculations only $C_{\gamma\gamma h}$, $C_{\gamma Zh}$ and $C_{WW\gamma}$ enter directly and therefore limits obtained on C_{WWh} and C_{ZZh} are also indirect. The limits on the strengths of the anomalous couplings are listed in Table IV. Since electroweak precision bounds on $\tilde{f}_i$ are the weakest,[5] in the table we compare bounds on couplings due to LHC data and EDMs. The comparison is presented for both the two parameter (2P) and three parameter (3P) nonzero cases. Since C_{WWZ} is proportional to $C_{WW\gamma}$, the limits on $C_{WW\gamma}$ can be easily translated to limits on C_{WWZ}. Looking at the LHC limits on the couplings we find that $C_{\gamma\gamma h}$ is the most constrained coupling. Also, the LHC limits in 2P and 3P cases are comparable. On the other hand the EDM limits on couplings in 2P case is always stronger than in 3P case. In 3P case the lower limits result from the three

---

[5]Although the EWP constraints are weaker in general, we find that the limits on C_{WWV} from EWP and LHC data are comparable in 2P case.

TABLE IV.   Limits on *CP*-odd coupling strengths from LHC data and EDM measurements for $\Lambda = 1$ TeV. 2P and 3P stand for two parameter nonzero and three parameter nonzero cases respectively.

Couplings	LHC data		EDM	
	2P case	3P case	2P case	3P case
$|C_{WWh}|$	0–60	0–60	0–0.17	0–55
$|C_{ZZh}|$	25–100	25–80	0.11–0.20	0.15–33
$|C_{\gamma\gamma h}|$	0–0.8	0–0.5	0–0.16	0.02–52
$|C_{\gamma Zh}|$	20–25	15–25	0.03–0.25	0.05–110
$|C_{WW\gamma}|$	0–40	15–40	0–0.15	0.02–47

parameter sets $\{\tilde{f}_B, \tilde{f}_{BB}, \tilde{f}_{BW}\}$ and $\{\tilde{f}_W, \tilde{f}_{WW}, \tilde{f}_{BW}\}$. The parameters of these sets are found to be very fine tuned. It is important to recall that in 3P EDM case, the parameters are varied in the range between -200 to 200. We find that as we increase this range, the maximum allowed values for couplings also increase. We would also like to point out that the correlations among *CP*-odd couplings are mostly similar to those found among *CP*-odd parameters.

The triple gauge boson couplings (TGCs) $WW\gamma$ and WWZ can also be constrained using the collider data on gauge boson pair production. Data from Tevatron and LHC are used mainly to constrain the *CP*-even anomalous couplings as the observables used are not sensitive to *CP*-odd couplings [85–90]. On the other hand, the experimental analyses at LEP which studied the angular distribution of final state particles are sensitive to *CP*-odd TGCs. A comparison between the *CP*-odd sector of TGC Lagrangian [54,91,92] and our effective Lagrangian (Eq. (2)) implies

$$\frac{C_{WW\gamma}}{\Lambda^2} = \frac{s_W}{m_W^2} \tilde{\kappa}_\gamma \tag{50}$$

$$\frac{C_{WWZ}}{\Lambda^2} = \frac{c_W}{m_W^2} \tilde{\kappa}_Z. \tag{51}$$

Using the relation between $C_{WW\gamma}$ and C_{WWZ} we get, $\tilde{\kappa}_Z = -t_W^2 \tilde{\kappa}_\gamma$. At 68% CL, the combined LEP limits on $\tilde{\kappa}_Z$ are [79]

$$-0.14 \leq \tilde{\kappa}_Z \leq -0.06. \tag{52}$$

These limits when translated on C_{WWZ} and $C_{WW\gamma}$ become,

$$-0.19 \leq \frac{C_{WWZ}}{\Lambda^2} [\text{TeV}^{-2}] \leq -0.08,$$

$$0.15 \leq \frac{C_{WW\gamma}}{\Lambda^2} [\text{TeV}^{-2}] \leq 0.36. \tag{53}$$

Note that these limits are comparable to the limits obtained from EDMs in 2P case, however, information on the sign of the couplings is also available.

Other than the VVh vertices considered in our analysis, quartic $VVhh$ vertices also arise out of gauge invariant *CP* violating operators. One can thus expect some correlated phenomenology from the trilinear and quartic interactions, since the former arise essentially on replacing one Higgs by its vacuum expectation value in the quartic terms. In the analysis presented in this work, the production and decay channels considered are not affected at tree level by such quartic $VVhh$ vertices. Thus in the context of the present analysis, any constraints on such quartic vertices from observed data are likely to be weaker than those obtained from the $VVh(V = W, Z, \gamma)$ effective interactions, since the quartic couplings would entail Higgs pair production. For example, the $VVhh$ vertex may contribute in addition to the hhh vertex toward a di-Higgs final state. However, one needs to wait for a large volume of data on Higgs pair production to see such correlated phenomena. In general, limits stronger than what we have obtained are not expected. Also, the contributions from such $VVhh$ *CP*-odd vertices to EDMs and EWP observables come at higher loop levels and thus are expected to be substantially weaker than what we have obtained for the trilinear terms.

It is a well-known fact that the observed baryon asymmetry in our universe cannot be explained by just the *CP*-violating phase of the Cabibbo-Kobayashi-Maskawa (CKM) matrix in the SM. The presence of additional sources of *CP*-violating operators arising from the anomalous VVh interactions may in principle explain the observed baryon asymmetry of the universe. However, a more careful scrutiny of this picture reveals that our *CP*-violating operators are not sufficient to trigger strongly the first order electroweak phase transition required for the baryogenesis. For this, one has to extend the Higgs sector of the SM by introducing new particles which couple to the Higgs boson and thus modify the Higgs potential such that it leads to a strongly first order electroweak phase transition [93].

VII. SUMMARY AND CONCLUSIONS

We have analyzed *CP*-odd $VVh(V = W, Z, \gamma)$ and $WWV(V = Z, \gamma)$ interactions in terms of gauge invariant dimension-6 operators, obtained as the artifacts of physics beyond the standard model. The most complete set, comprising five gauge-Higgs operators, has been taken into account. We have derived constraints on the coefficients of such operators using electroweak precision data, LHC data on Higgs and limits on the electric dipole moments of the neutron and the electron. With Λ as the scale suppressing the *CP*-violating operators, precision parameters as well as LHC observables receive contributions $\sim 1/\Lambda^4$ from the *CP*-odd couplings, while contributions $\sim 1/\Lambda^2$ to EDM observables are expected. The constraints obtained from the S, T and U parameters are the weakest, while the bounds from EDMs are the strongest with two nonvanishing operators. The global analysis of

Higgs data from the LHC puts stronger constraints on those *CP*-odd effective couplings which contribute to $h \to \gamma\gamma$, as compared to those which do not. We also indicate situations where large values of certain couplings are allowed by all constraints, when they appear in combination. The constraints coming from LEP on *CP*-odd form factors $C_{WW\gamma}$ and C_{WWZ} are consistent with our limits obtained from EDMs in the case when any two out of five parameters are nonzero. It may be of interest to find out new physics scenarios where, by integrating out heavy degrees of freedom, one may arrive at large correlated values of such operators. In a subsequent work, [94] we hope to discuss some observables that may help one in probing these operators in the 13 and 14 TeV LHC runs.

ACKNOWLEDGMENTS

APPENDIX: GAUGE BOSON TWO-POINT FUNCTIONS IN PRESENCE OF *CP*-ODD COUPLINGS

We define the two-point function for electroweak gauge bosons V_1 and V_2 as,

$$\Pi^{\mu\nu}_{V_1 V_2}(p^2) = g^{\mu\nu}\Pi_{V_1 V_2}(p^2) + p^\mu p^\nu \tilde{\Pi}_{V_1 V_2}(p^2). \quad (A1)$$

In electroweak precision observables only $\Pi_{V_1 V_2}(p^2)$ contribute. Below we give their expressions due to *CP*-odd couplings in terms of one-loop scalar functions A_0 and B_0.

$$\begin{aligned}
\Pi_{\gamma\gamma}(p^2) = \frac{g^2 m_W^2}{18\Lambda^4}(&3p^2(C_{\gamma\gamma h}^2(2m_h^2 - p^2)B_0(p^2, 0, m_h^2) - 2C_{WW\gamma}^2(2m_W^2 + p^2)B_0(p^2, m_W^2, m_W^2) \\
&+ C_{\gamma Zh}^2 A_0(m_Z^2) + 4C_{WW\gamma}^2 A_0(m_W^2)) - 3C_{\gamma\gamma h}^2 m_h^4 B_0(p^2, 0, m_h^2) - 3C_{\gamma Zh}^2(m_h^4 - 2m_h^2(m_Z^2 + p^2) \\
&+ (m_Z^2 - p^2)^2)B_0(p^2, m_Z^2, m_h^2) + 3A_0(m_h^2)(C_{\gamma\gamma h}^2(m_h^2 + p^2) + C_{\gamma Zh}^2(m_h^2 - m_Z^2 + p^2)) \\
&+ 3C_{\gamma Zh}^2 A_0(m_Z^2)(m_Z^2 - m_h^2) + p^2(7C_{\gamma\gamma h}^2(p^2 - 3m_h^2) + 7C_{\gamma Zh}^2(p^2 - 3(m_h^2 + m_Z^2)) \\
&+ 2C_{WW\gamma}^2(12m_W^2 + 7p^2))),
\end{aligned} \quad (A2)$$

$$\begin{aligned}
\Pi_{\gamma Z}(p^2) = \frac{g^2 m_W^2}{18\Lambda^4}(&-3C_{\gamma\gamma h}C_{\gamma Zh}(m_h^2 - p^2)^2 B_0(p^2, 0, m_h^2) - 3C_{\gamma Zh}C_{ZZh}(m_h^4 - 2m_h^2(m_Z^2 + p^2) \\
&+ (m_Z^2 - p^2)^2)B_0(p^2, m_Z^2, m_h^2) - 6C_{WW\gamma}C_{WWZ}p^2(2m_W^2 + p^2)B_0(p^2, m_W^2, m_W^2) \\
&+ 3C_{\gamma Zh}A_0(m_h^2)(C_{\gamma\gamma h}(m_h^2 + p^2) + C_{ZZh}(m_h^2 - m_Z^2 + p^2)) + 3C_{\gamma Zh}C_{ZZh}A_0(m_Z^2)(-m_h^2 + m_Z^2 + p^2) \\
&+ 12C_{WW\gamma}C_{WWZ}p^2 A_0(m_W^2) + p^2(7p^2(C_{\gamma Zh}(C_{\gamma\gamma h} + C_{ZZh}) \\
&+ 2C_{WW\gamma}C_{WWZ}) - 21C_{\gamma Zh}(m_h^2(C_{\gamma\gamma h} + C_{ZZh}) + C_{ZZh}m_Z^2) + 24C_{WW\gamma}C_{WWZ}m_W^2)),
\end{aligned} \quad (A3)$$

$$\begin{aligned}
\Pi_{ZZ}(p^2) = \frac{g^2 m_W^2}{18\Lambda^4}(&3p^2(C_{\gamma Zh}^2(2m_h^2 - p^2)B_0(p^2, 0, m_h^2) - 2C_{WWZ}^2(2m_W^2 + p^2)B_0(p^2, m_W^2, m_W^2) \\
&+ 4C_{WWZ}^2 A_0(m_W^2) + C_{ZZh}^2 A_0(m_Z^2)) - 3C_{\gamma Zh}^2 m_h^4 B_0(p^2, 0, m_h^2) - 3C_{ZZh}^2(m_h^4 - 2m_h^2(m_Z^2 + p^2) \\
&+ (m_Z^2 - p^2)^2)B_0(p^2, m_Z^2, m_h^2) + 3A_0(m_h^2)(C_{\gamma Zh}^2(m_h^2 + p^2) + C_{ZZh}^2(m_h^2 - m_Z^2 + p^2)) \\
&+ 3C_{ZZh}^2 A_0(m_Z^2)(m_Z^2 - m_h^2) + p^2(7C_{\gamma Zh}^2(p^2 - 3m_h^2) + 2C_{WWZ}^2(12m_W^2 + 7p^2) \\
&+ 7C_{ZZh}^2(p^2 - 3(m_h^2 + m_Z^2)))),
\end{aligned} \quad (A4)$$

$$
\begin{aligned}
\Pi_{WW}(p^2) = \frac{g^2 m_W^2}{18\Lambda^4 p^2} & (3(-C_{WW\gamma}^2(m_W^2 - p^2)^2(m_W^2 + p^2)B_0(p^2, m_W^2, 0) + C_{WWh}^2(-p^2)(m_h^4 \\
& - 2m_h^2(m_W^2 + p^2) + (m_W^2 - p^2)^2)B_0(p^2, m_W^2, m_h^2) - C_{WWZ}^2(m_W^6 - m_W^4(2m_Z^2 + p^2) \\
& + m_W^2(m_Z^4 + 8m_Z^2 p^2 - (p^2)^2) + p^2(m_Z^2 - p^2)^2)B_0(p^2, m_W^2, m_Z^2) - C_{WWZ}^2 A_0(m_Z^2)(m_W^2 + p^2)(m_W^2 - m_Z^2 - p^2)) \\
& + 3A_0(m_W^2)(C_{WW\gamma}^2(m_W^4 - 10m_W^2 p^2 + (p^2)^2) + C_{WWh}^2 p^2(-m_h^2 + m_W^2 + p^2) \\
& + C_{WWZ}^2(m_W^4 - m_W^2(m_Z^2 + 10p^2) + p^2(p^2 - m_Z^2))) + 3C_{WWh}^2 p^2 A_0(m_h^2)(m_h^2 - m_W^2 + p^2) \\
& + p^2(C_{WW\gamma}^2(87m_W^4 - 14m_W^2 p^2 + 7(p^2)^2) + 7C_{WWh}^2 p^2(p^2 - 3(m_h^2 + m_W^2)) \\
& + C_{WWZ}^2(-7p^2(2m_W^2 + 3m_Z^2) + 87m_W^2(m_W^2 + m_Z^2) + 7(p^2)^2))).
\end{aligned} \tag{A5}
$$

Out of these, $\Pi_{\gamma\gamma}$, $\Pi_{\gamma Z}$ and Π_{ZZ} vanish at $p^2 = 0$. Note that in Π_{WW} there is an overall $1/p^2$ dependence. We would like to mention that both Π_{WW} and its derivative converge smoothly in $p^2 \to 0$ limit. The one-loop scalar functions in $n = 4 - 2\epsilon$ dimensions are given by,

$$
\begin{aligned}
A_0(m_0^2) &= \int \frac{d^n l}{(2\pi)^n} \frac{1}{l^2 - m_0^2} \\
&\equiv \frac{1}{16\pi^2} m_0^2 \left[\frac{1}{\epsilon} + 1 - \ln(m_0^2) \right],
\end{aligned} \tag{A6}
$$

$$
\begin{aligned}
B_0(p^2, m_0^2, m_1^2) &= \int \frac{d^n l}{(2\pi)^n} \frac{1}{(l^2 - m_0^2)((l+p)^2 - m_1^2)} \\
&\equiv \frac{1}{16\pi^2} \left[\frac{1}{\epsilon} - \Delta(p^2, m_0^2, m_1^2) \right],
\end{aligned} \tag{A7}
$$

where,

$$
\begin{aligned}
\Delta(p^2, m_0^2, m_1^2) = \int_0^1 dx \ln[&-x(1-x)p^2 \\
&+ x(m_1^2 - m_0^2) + m_0^2].
\end{aligned} \tag{A8}
$$

This form is suitable for computing B_0 and its derivative with respect to p^2 at $p^2 = 0$, which we require to calculate S, T and U parameters discussed in Sec. III.

[1] G. Aad *et al.* (ATLAS Collaboration), Observation of a new particle in the search for the standard model Higgs boson with the ATLAS detector at the LHC, Phys. Lett. B **716**, 1 (2012).

[2] S. Chatrchyan *et al.* (CMS Collaboration), Observation of a new boson at a mass of 125 GeV with the CMS experiment at the LHC, Phys. Lett. B **716**, 30 (2012).

[3] P. P. Giardino, K. Kannike, M. Raidal, and A. Strumia, Reconstructing Higgs boson properties from the LHC and Tevatron data, J. High Energy Phys. 06 (2012) 117.

[4] M. Klute, R. Lafaye, T. Plehn, M. Rauch, and D. Zerwas, Measuring Higgs Couplings from LHC Data, Phys. Rev. Lett. **109**, 101801 (2012).

[5] S. Banerjee, S. Mukhopadhyay, and B. Mukhopadhyaya, New Higgs interactions and recent data from the LHC and the Tevatron, J. High Energy Phys. 10 (2012) 062.

[6] M. B. Einhorn and J. Wudka, Higgs-boson couplings beyond the standard model, Nucl. Phys. **B877**, 792 (2013).

[7] M. Baak, J. Cúth, J. Haller, A. Hoecker, R. Kogler, K. Mönig, M. Schott, and J. Stelzer, The global electroweak fit at NNLO and prospects for the LHC and ILC, Eur. Phys. J. C **74**, 3046 (2014).

[8] W. Buchmuller and D. Wyler, Effective Lagrangian analysis of new interactions and flavor conservation, Nucl. Phys. **B268**, 621 (1986).

[9] B. Grzadkowski, M. Iskrzynski, M. Misiak, and J. Rosiek, Dimension-six terms in the standard model Lagrangian, J. High Energy Phys. 10 (2010) 085.

[10] J. R. Espinosa, C. Grojean, M. Muhlleitner, and M. Trott, Fingerprinting Higgs suspects at the LHC, J. High Energy Phys. 05 (2012) 097.

[11] A. Azatov, R. Contino, and J. Galloway, Model-independent bounds on a light Higgs, J. High Energy Phys. 04 (2012) 127; 04 (2013) 140.

[12] R. Contino, M. Ghezzi, C. Grojean, M. Muhlleitner, and M. Spira, Effective Lagrangian for a light Higgs-like scalar, J. High Energy Phys. 07 (2013) 035.

[13] F. Maltoni, K. Mawatari, and M. Zaro, Higgs characterisation via vector-boson fusion and associated production: NLO and parton-shower effects, Eur. Phys. J. C **74**, 2710 (2014).

[14] E. Masso, An effective guide to beyond the standard model physics, J. High Energy Phys. 10 (2014) 128.

[15] A. Falkowski, Effective field theory approach to LHC Higgs data, arXiv:1505.00046.

[16] M. C. Gonzalez-Garcia, Anomalous Higgs couplings, Int. J. Mod. Phys. A **14**, 3121 (1999).

[17] T. Han and J. Jiang, CP violating *ZZh* coupling at $e^+ e^-$ linear colliders, Phys. Rev. D **63**, 096007 (2001).

[18] T. Plehn, D. L. Rainwater, and D. Zeppenfeld, Determining the Structure of Higgs Couplings at the LHC, Phys. Rev. Lett. **88**, 051801 (2002).

[19] V. Barger, T. Han, P. Langacker, B. McElrath, and P. Zerwas, Effects of genuine dimension-six Higgs operators, Phys. Rev. D **67**, 115001 (2003).

[20] S. S. Biswal, R. M. Godbole, R. K. Singh, and D. Choudhury, Signatures of anomalous VVH interactions at a linear collider, Phys. Rev. D **73**, 035001 (2006); **74**, 039904 (2006).

[21] T. Han, Y. P. Kuang, and B. Zhang, Anomalous gauge couplings of the Higgs boson at high energy photon colliders, Phys. Rev. D **73**, 055010 (2006).

[22] R. M. Godbole, S. Kraml, S. D. Rindani, and R. K. Singh, Probing *CP*-violating Higgs contributions in $\gamma\gamma \to f\bar{f}$ through fermion polarization, Phys. Rev. D **74**, 095006 (2006); **74**, 119901 (2006).

[23] R. M. Godbole, D. J. Miller, and M. M. Muhlleitner, Aspects of *CP* violation in the H ZZ coupling at the LHC, J. High Energy Phys. 12 (2007) 031.

[24] S. S. Biswal and R. M. Godbole, Use of transverse beam polarization to probe anomalous VVH interactions at a Linear Collider, Phys. Lett. B **680**, 81 (2009).

[25] N. D. Christensen, T. Han, and Y. Li, Testing *CP* violation in ZZH interactions at the LHC, Phys. Lett. B **693**, 28 (2010).

[26] N. Desai, D. K. Ghosh, and B. Mukhopadhyaya, *CP*-violating HWW couplings at the Large Hadron Collider, Phys. Rev. D **83**, 113004 (2011).

[27] A. Freitas and P. Schwaller, Higgs *CP* properties from early LHC data, Phys. Rev. D **87**, 055014 (2013).

[28] W. Dekens and J. de Vries, Renormalization group running of dimension-six sources of parity and time-reversal violation, J. High Energy Phys. 05 (2013) 149.

[29] C. Y. Chen, S. Dawson, and C. Zhang, Electroweak effective operators and Higgs physics, Phys. Rev. D **89**, 015016 (2014).

[30] S. S. Biswal, R. M. Godbole, B. Mellado, and S. Raychaudhuri, Azimuthal Angle Probe of Anomalous *HWW* Couplings at a High Energy ep Collider, Phys. Rev. Lett. **109**, 261801 (2012).

[31] I. Low, J. Lykken, and G. Shaughnessy, Have we observed the Higgs (imposter)?, Phys. Rev. D **86**, 093012 (2012).

[32] E. Mass and V. Sanz, Limits on anomalous couplings of the Higgs boson to electroweak gauge bosons from LEP and the LHC, Phys. Rev. D **87**, 033001 (2013).

[33] A. Djouadi and G. Moreau, The couplings of the Higgs boson and its *CP* properties from fits of the signal strengths and their ratios at the $7 + 8$ TeV LHC, Eur. Phys. J. C **73**, 2512 (2013).

[34] I. T. Cakir, O. Cakir, A. Senol, and A. T. Tasci, Probing anomalous HZZ couplings at the LHeC, Mod. Phys. Lett. A **28**, 1350142 (2013).

[35] R. Godbole, D. J. Miller, K. Mohan, and C. D. White, Boosting Higgs *CP* properties via VH production at the Large Hadron Collider, Phys. Lett. B **730**, 275 (2014).

[36] S. Banerjee, S. Mukhopadhyay, and B. Mukhopadhyaya, Higher dimensional operators and the LHC Higgs data: The role of modified kinematics, Phys. Rev. D **89**, 053010 (2014).

[37] I. Anderson, S. Bolognesi, F. Caola, Y. Gao, A. V. Gritsan, C. B. Martin, K. Melnikov, M. Schulze *et al.*, Constraining anomalous HVV interactions at proton and lepton colliders, Phys. Rev. D **89**, 035007 (2014).

[38] R. M. Godbole, D. J. Miller, K. A. Mohan, and C. D. White, Jet substructure and probes of *CP* violation in Vh production, J. High Energy Phys. 04 (2015) 103.

[39] V. Khachatryan *et al.* (CMS Collaboration), Constraints on the spin-parity and anomalous HVV couplings of the Higgs boson in proton collisions at 7 and 8 TeV, Phys. Rev. D **92**, 012004 (2015).

[40] J. Ellis, V. Sanz, and T. You, Complete Higgs sector constraints on dimension-6 operators, J. High Energy Phys. 07 (2014) 036.

[41] Y. Chen, A. Falkowski, I. Low, and R. Vega-Morales, New observables for *CP* violation in Higgs decays, Phys. Rev. D **90**, 113006 (2014).

[42] A. V. Manohar and M. B. Wise, Modifications to the properties of the Higgs boson, Phys. Lett. B **636**, 107 (2006).

[43] T. Corbett, O. J. P. Eboli, J. Gonzalez-Fraile, and M. C. Gonzalez-Garcia, Constraining anomalous Higgs interactions, Phys. Rev. D **86**, 075013 (2012).

[44] T. Corbett, O. J. P. Eboli, J. Gonzalez-Fraile, and M. C. Gonzalez-Garcia, Robust determination of the Higgs couplings: Power to the data, Phys. Rev. D **87**, 015022 (2013).

[45] W.-F. Chang, W.-P. Pan, and F. Xu, Effective gauge-Higgs operators analysis of new physics associated with the Higgs boson, Phys. Rev. D **88**, 033004 (2013).

[46] B. Gripaios and D. Sutherland, Searches for *CP*-violating dimension-6 electroweak gauge boson operators, Phys. Rev. D **89**, 076004 (2014).

[47] H. Belusca-Maito, Effective Higgs Lagrangian and Constraints on Higgs Couplings, arXiv:1404.5343.

[48] A. Falkowski and F. Riva, Model-independent precision constraints on dimension-6 operators, J. High Energy Phys. 02 (2015) 039.

[49] D. McKeen, M. Pospelov, and A. Ritz, Modified Higgs branching ratios versus *CP* and lepton flavor violation, Phys. Rev. D **86**, 113004 (2012).

[50] K. A. Olive *et al.* (Particle Data Group Collaboration), Review of particle physics, Chin. Phys. C **38**, 090001 (2014).

[51] A. D. Sakharov, Violation of CP invariance, c asymmetry, and baryon asymmetry of the universe, Pis'ma Zh. Eksp. Teor. Fiz. **5**, 32 (1967) [JETP Lett. **5**, 24 (1967)]; Usp. Fiz. Nauk **161**, 61 (1991) [Sov. Phys. Usp. **34**, 392 (1991)].

[52] A. Riotto, Theories of Baryogenesis, arXiv:hep-ph/9807454.

[53] M. B. Voloshin, CP violation in Higgs diphoton decay in models with vectorlike heavy fermions, Phys. Rev. D **86**, 093016 (2012).

[54] M. B. Gavela, J. Gonzalez-Fraile, M. C. Gonzalez-Garcia, L. Merlo, S. Rigolin, and J. Yepes, CP violation with a dynamical Higgs, J. High Energy Phys. 10 (2014) 44.

[55] J. Yepes, R. Kunming, and J. Shu, CP violation from spin-1 resonances in a left-right dynamical Higgs context, arXiv:1507.04745.

[56] C. S. Lim, CP violation in higher dimensional theories, Phys. Lett. B **256**, 233 (1991).

[57] C. S. Lim, N. Maru, and K. Nishiwaki, CP violation due to compactification, Phys. Rev. D **81**, 076006 (2010).

[58] R. D. Peccei and H. R. Quinn, CP Conservation in the Presence of Instantons, Phys. Rev. Lett. **38**, 1440 (1977).

[59] R. D. Peccei and H. R. Quinn, Constraints imposed by CP conservation in the presence of instantons, Phys. Rev. D **16**, 1791 (1977).

[60] M. E. Peskin and T. Takeuchi, Estimation of oblique electroweak corrections, Phys. Rev. D **46**, 381 (1992).

[61] J. Alwall, R. Frederix, S. Frixione, V. Hirschi, F. Maltoni, O. Mattelaer, H.-S. Shao, T. Stelzer, P. Torrielli, and M. Zaro, The automated computation of tree-level and next-to-leading order differential cross sections, and their matching to parton shower simulations, J. High Energy Phys. 07 (2014) 079.

[62] N. D. Christensen and C. Duhr, FeynRules - Feynman rules made easy, Comput. Phys. Commun. **180**, 1614 (2009).

[63] J. Pumplin, D. R. Stump, J. Huston, H. L. Lai, P. M. Nadolsky, and W. K. Tung, New generation of parton distributions with uncertainties from global QCD analysis, J. High Energy Phys. 07 (2002) 012.

[64] https://twiki.cern.ch/twiki/bin/view/LHCPhysics/CrossSections

[65] S. Chatrchyan *et al.* (CMS Collaboration), Search for a Higgs boson decaying into a Z and a photon in pp collisions at $\sqrt{s} = 7$ and 8 TeV, Phys. Lett. B **726**, 587 (2013).

[66] G. Aad *et al.* (ATLAS Collaboration), Search for Higgs boson decays to a photon and a Z boson in pp collisions at $\sqrt{s} = 7$ and 8 TeV with the ATLAS detector, Phys. Lett. B **732**, 8 (2014).

[67] G. Aad *et al.* (ATLAS Collaboration), Measurement of Higgs boson production in the diphoton decay channel in pp collisions at center-of-mass energies of 7 and 8 TeV with the ATLAS detector, Phys. Rev. D **90**, 112015 (2014).

[68] V. Khachatryan *et al.* (CMS Collaboration), Observation of the diphoton decay of the Higgs boson and measurement of its properties, Eur. Phys. J. C **74**, 3076 (2014).

[69] G. Aad *et al.* (ATLAS Collaboration), Measurements of Higgs boson production and couplings in the four-lepton channel in pp collisions at center-of-mass energies of 7 and 8 TeV with the ATLAS detector, Phys. Rev. D **91**, 012006 (2015).

[70] S. Chatrchyan *et al.* (CMS Collaboration), Measurement of the properties of a Higgs boson in the four-lepton final state, Phys. Rev. D **89**, 092007 (2014).

[71] ATLAS-CONF-2014-060.

[72] S. Chatrchyan *et al.* (CMS Collaboration), Measurement of Higgs boson production and properties in the WW decay channel with leptonic final states, J. High Energy Phys. 01 (2014) 096.

[73] V. Khachatryan *et al.* (CMS Collaboration), Constraints on the Higgs boson width from off-shell production and decay to Z-boson pairs, Phys. Lett. B **736**, 64 (2014).

[74] C. Englert, A. Freitas, M. M. Mhlleitner, T. Plehn, M. Rauch, M. Spira, and K. Walz, Precision measurements of Higgs couplings: Implications for new physics scales, J. Phys. G **41**, 113001 (2014).

[75] M. Pospelov and A. Ritz, Electric dipole moments as probes of new physics, Ann. Phys. (Amsterdam) **318**, 119 (2005).

[76] J. Engel, M. J. Ramsey-Musolf, and U. van Kolck, Electric dipole moments of nucleons, nuclei, and atoms: The standard model and beyond, Prog. Part. Nucl. Phys. **71**, 21 (2013).

[77] A. Czarnecki and B. Krause, Neutron Electric Dipole Moment in the Standard Model: Valence Quark Contributions, Phys. Rev. Lett. **78**, 4339 (1997).

[78] J. Baron *et al.* (ACME Collaboration), Order of magnitude smaller limit on the electric dipole moment of the electron, Science **343**, 269 (2014).

[79] J. Beringer *et al.* (Particle Data Group Collaboration), Review of particle physics (RPP), Phys. Rev. D **86**, 010001 (2012).

[80] C. A. Baker, D. D. Doyle, P. Geltenbort, K. Green, M. G. D. van der Grinten, P. G. Harris, P. Iaydjiev, S. N. Ivanov *et al.*, An Improved Experimental Limit on the Electric Dipole Moment of the Neutron, Phys. Rev. Lett. **97**, 131801 (2006).

[81] C. Dib, A. Faessler, T. Gutsche, S. Kovalenko, J. Kuckei, V. E. Lyubovitskij, and K. Pumsa-ard, The neutron electric dipole form-factor in the perturbative chiral quark model, J. Phys. G **32**, 547 (2006).

[82] J. C. Peng, Neutron electric dipole moment experiments, Mod. Phys. Lett. A **23**, 1397 (2008).

[83] T. M. Ito, Plans for a neutron EDM experiment at SNS, J. Phys. Conf. Ser. **69**, 012037 (2007).

[84] M. Raidal *et al.*, Flavour physics of leptons and dipole moments, Eur. Phys. J. C **57**, 13 (2008).

[85] H. T. Diehl (CDF and D0 Collaborations), Vector Boson Pair Production and Trilinear Gauge Boson Couplings - Results From the Tevatron, arXiv:hep-ex/9810006.

[86] V. M. Abazov *et al.* (D0 Collaboration), $W\gamma$ Production and Limits on Anomalous $WW\gamma$ Couplings in $p\bar{p}$ Collisions, Phys. Rev. Lett. **107**, 241803 (2011).

[87] G. Aad *et al.* (ATLAS Collaboration), Measurement of WZ production in proton-proton collisions at $\sqrt{s} = 7$ TeV with the ATLAS detector, Eur. Phys. J. C **72**, 2173 (2012).

[88] G. Aad *et al.* (ATLAS Collaboration), Measurement of W^+W^- production in pp collisions at $\sqrt{s} = 7$ TeV with the ATLAS detector and limits on anomalous WWZ and WW couplings, Phys. Rev. D **87**, 112001 (2013); **88**, 079906(E) (2013).

[89] S. Chatrchyan *et al.* (CMS Collaboration), Measurement of the W^+W^- cross section in pp collisions at $\sqrt{s} = 7$ TeV and limits on anomalous $WW\gamma$ and WWZ couplings, Eur. Phys. J. C **73**, 2610 (2013).

[90] S. Chatrchyan *et al.* (CMS Collaboration), Measurement of the $W\gamma$ and $Z\gamma$ inclusive cross sections in pp collisions at $\sqrt{s} = 7$ TeV and limits on anomalous triple gauge boson couplings, Phys. Rev. D **89**, 092005 (2014).

[91] K. Hagiwara, R. D. Peccei, D. Zeppenfeld, and K. Hikasa, Probing the weak boson sector in $e^+e^- \rightarrow W^+W^-$, Nucl. Phys. **B282**, 253 (1987).

[92] S. Dawson, S. K. Gupta, and G. Valencia, CP violating anomalous couplings in $W\gamma$ and $Z\gamma$ production at the LHC, Phys. Rev. D **88**, 035008 (2013).

[93] D. E. Morrissey and M. J. Ramsey-Musolf, Electroweak baryogenesis, New J. Phys. **14**, 125003,(2012); Electroweak baryogenesis, arXiv:1206.2942 and references therein.

[94] S. Dwivedi, D. K. Ghosh, B. Mukhopadhyaya, and A. Shivaji (to be published).